Flow sensing with arrays of fibre-optic whisker sensors

Raphael A. Glick

Thesis submitted for the degree of Doctor of Philosophy

City, University of London

Department of Engineering

October 2024

Declaration

I, Raphael Glick confirm that the work presented in this thesis is my own. Where information has been derived from other sources, I confirm that this has been indicated in the thesis

There is no embargo, commercial or related to any funding received, preventing the immediate publication of the contents of this thesis, nor is there any material included in this thesis that infringes Copyright or Data Protection Regulations.

Contents

List of Figures

List of Tables

Acknowledgements

Firstly, I would like to extend my gratitude to Prof. Christoph Brücker for his continuous support, guidance, and insight throughout my studies, without which this research would not have been possible. I would like to thank Prof. Kenneth Grattan for his guidance, assistance with publications, and insights into the field of Optics. I would like to thank Dr Matthias Fabian and Dr Sankhyabrata Bandyopadhyay for their time, patience, and guidance while helping me through the delicate process of manufacturing glass fibre sensors. I would like to thank Dr Muthukumar Muthuramalingam for his support, for his work on whiskers, and for his work on the water tunnel models, all of which made my project possible. I would like to thank Keith Pamment and the rest of the workshop staff for their time, effort, and advice, while manufacturing the many parts needed along the way. I would like to thank Dr Edward Tallboys for introducing me to the world of research, and for encouraging me to push myself to undertake further study. I would like to thank the rest of my research group for their support, assurances, and insights over the course of my study. Lastly I would like to thank my parents, siblings, and friends, without whom I would not have maintained my sanity throughout the various pandemic related crises.

I would also like to acknowledge the funding received from the DFG, The Royal Academy of Engineering, and BAE Systems, which contributed to various stages of the project.

Abstract

In nature, sensing critical flow events or flow signatures is often achieved through a coupled interaction between a fluid and arrays of slender flexible beams, such as whiskers and wind-hairs. Behavioural research on live sea lions has shown that they are able to discern the direction of oncoming vortices, even when they impact the animal's whiskers contralaterally. These experiments show that the whiskers coupled with the animal's neural processing can detect the direction of arrival of a flow event, just using information from the whiskers on one side of the head. Therefore, it is hypothesized that in highly noisy environments, important information is gained from the time differences between whisker stimulation. Herein, numerous iterations of bio-mimetic sensors, array designs, and the decoding of the relationship between the sensors are investigated.

A model sea lion head with slender plastic optical fibre whiskers was subjected to a mean flow with overlaid turbulent structures generated in the wake of a cylinder. A motion tracking camera observed the array of fibres to track the bending deformations of the fibres. The characteristic signature of the passage of a vortex core, a jerk-like motion of the whisker, is apparent in the leading sensor, and in the response of subsequent sensors, even in the wake of the first whisker. Cross-correlation of the time domain of the bending signal from pairs of whiskers proves that the detection of vortices and their passage along the animal's head is possible even in noisy environments.

Following these observations, a theoretical model for tracking the path of an unknown flow disturbance is devised, adapted from multilateration principles used for electromagnetic and acoustic source localisation. The model focuses on tracking a signal of unknown size, speed, and direction as it passes the array using the time signatures and known distances between triplets of disturbed whiskers. The model is tested against experimental studies on the model seal head, and a simple 2D

array with regular spacing. The results validate the principle behind the model, and highlight the sensitivity of the model to the array layout and spacing. An optimised array was produced based on these findings, with tuned array spacing, sensor length, and a new layout minimising co-linearity between the sensors. Further tests validated the efficacy of the design with a mean output angle RMSE of 1.9°.

Finally, a new whisker sensor design is presented, using the enhanced sensitivity and performance of fibre Bragg Grating (FBG) engraved optical stress sensors. Its performance is evaluated against the original sensors, with the added benefit of removing the tracking camera from the process. The performance and improved sensitivity of these FBG-based fibre-optic whiskers is shown to produce reliable direction of arrival and velocity estimations, at a typical SNR of around 2dB. The FBG sensors correct for disruptive variations in temperature using a second grating at the whisker tip, positioned at the point with the least bending stress, allowing for isolated bending stress measurements and identification of the hydrodynamic disturbances of interest.

The study herein further develops our understanding of flow sensing systems and how they can overcome high background noise levels with the application of the correlation principle. Further, the study explores array design principles and sensitivities, covering several methods to improve the signal output that have been trialled and shown to improve the performance of the array, with further recommendations made for various applications. Lastly a new sensor design is presented, with the objective of broadening deployment options while maximising sensitivity, expanding the range of suitable applications for whisker sensors.

Chapter 1

Introduction

In recent years, the study of Biomimetics has produced a large number of innovations, across many disciplines, throughout the world of science and technology. Elegant and unexpected solutions to complex problems can be found by taking inspiration from the path forged by nature. Here we have entered a large problem space, with many competing approaches, all with strengths and drawbacks. There is no shortage of competing sensors that can contribute to sensing the world around us, but within the space of fluid flow, specifically hydrodynamics, there is space for innovation around sensors that 'feel' the flow moving around themselves. Any sensor within a bow wake, and especially within the boundary layer of a larger object, is potentially missing useful information carried within the free stream. The whiskers of pinnipeds seem uniquely capable of picking up this information, usually found in the form of wake disturbances left behind by small fish.

Other biomimetic centred approaches to sensors have looked to the whisker use of small mammals, or the lateral line systems used by fish, both of which aid their owners to navigate their respective environments.

Gomez et al. (Gomez et al. 2024) explore using a large array of 32 whiskers to mimic naked mole rats who depend heavily on their whiskers to navigate their subterranean environments. The array was designed for 3D mapping in unstructured environments, with the walls or obstacles moving a magnet based sensor at the root of the whisker. The array was successful in mapping 3D environments when attached to a range of robotic platforms. Deer and Pounds (Deer & Pounds 2019) used small scale MEMS barometer based arrays of plastic whisker sensors. While also for robotic use, they are used here as a pre-contact, collision warning system for autonomous vehicles, in particular, flying drones. The lightweight sensor package could be used by very small drones to detect gusts or objects that could restrict navigation.

Liu et al. (Liu et al. 2024) developed a hydrodynamic sensor based off of the lateral line systems of fish (Bleckmann & Zelick 2009). They used triboelectric dynamic pressure sensors inside of a mounting case to build an array of sensors that could detect the motion of a nearby robotic vessel. Using a sparse array and long time frames, the array could observe the movement of the vessel.

Muthuramalingam and Brücker(Muthuramalingam & Brücker 2019) developed a whisker array mounted to a model sea lion to predict the position of hydrodynamic disturbances. Here back-lit optical fibres were tracked optically to monitor the motion of the whiskers. They observed a slip stick response similar to small mammals that they used to suggest that it was the time derivative of the whiskers motion that influenced the seals tracking.

These areas of study produced promising results, and helped shape our approach to taking on artificial pinniped sensors. Our approach has focused on capitalising on the remarkable performance demonstrated by pinnipeds' hunting behaviour. The biology is clear; much time and effort has already been spent investigating the abilities of pinnipeds. Pinnipeds' have the ability to not only track the wake of small fishes significant periods of time beyond when a fish has passed by, but also to discern, with remarkable reliability, the direction in which their prey was moving. It is clear therefore that if we can capture the mechanism through which the pinnipeds' whiskers function, we would be able to create a powerful hydrodynamic sensor, with impressive tracking abilities of its own.

This thesis will therefore focus on the development of a biomimetic whisker sensor system, that can both track hydrodynamic disturbances, and be sufficiently versatile such that it could be deployed outside of idealised laboratory conditions. The following sections will discuss some of the key concepts that govern the success of our time-based whisker sensor arrays.

1.1 Whisker-Vortex FSI (VIV & WIV)

Vortex Induced Vibration (VIV) and Wake Induced Vibration (WIV) are the self-induced, and sympathetically induced vibrations of a whisker sensor respectively.

These vibrations occur in response to the whisker shedding vortices from alternate sides into its own wake (VIV) and as sympathetic vibrations in response to the whisker experiencing dynamic loads in the wake of another body shedding vortices from alternating sides (WIV).

Multiple groups (Valdivia y Alvarado et al. 2012, Lyons et al. 2020) have studied how the VIV of a sensor can be minimised via altering the design of the whisker, often taking cues from nature where elliptical-cross sections, undulating morphology, and tapered whiskers, are common methods for reducing noise from both VIV and other sources. Further studies investigate how such design elements affect the VIV and characterise the effect of these features on the response of a sensor (Leclercq & de Langre 2018, Zheng 2022). Whilst the conclusions of these studies make it clear that more complex whisker geometry can offer a noticeable reduction in noise levels, the 3D printed artificial whiskers produced for those studies were oversized compared to natural whiskers and sacrificed mimicking the mechanical properties of the natural whiskers. The latter was perceived to be more critical to this study, and it could be shown that the VIV vibrations were outside the range of the frequencies to be measured in the study. Therefore, the additional noise from using circular whiskers was deemed acceptable, preferring instead to place emphasis on the mechanical properties of the whiskers more closely mimicking natural whiskers.

A further consequence of not taking measures to limit VIV, is the increased likelihood and/or strength of WIVs. The concern surrounding WIV is that in an array of similar whiskers, each whisker will have a similar shedding frequency, resulting in the wake of an upstream whisker being exacerbated through resonant vibration of subsequent whiskers downstream (Zheng et al. 2023). In nature this is partially offset by the differing lengths of the whiskers slightly shifting the natural frequency of each shedding, but in general it is the whisker diameter that prescribes the vibration frequency as per

$$F_w = St\frac{V}{D_w} \tag{1.1}$$

Where whisker shedding frequency, 'F_w', is calculated from the characteristic length, 'D_w', which in this case in the whisker diameter.

This effect can still be offset by spacing the sensors out such that the wake of the upstream whisker is diminished before it reaches the next whisker in its path. This is the strategy employed in the early arrays used herein (see fig. 3.4b), but later studies found the inter-whisker spacing excessively large for detecting the target dimension vortices. The smaller array spacing used thereafter did suffer increased WIVs, but the relatively high frequency allowed for this motion to be largely filtered out. Further, the bearing calculations described later on herein, selected whisker groupings that minimised the co-linearity of the grouped sensors, as this anyway provided the best results for the employed tracking method. This had a secondary benefit of reducing the impact of whisker induced WIV, as sensors directly behind one another, where the effect of WIVs would be at its greatest, were not directly compared.

Managing the WIV component was made more difficult due to one of the main stimuli that the array was tasked with detecting, being the wake behind a cylinder. Thus, whiskers experiencing WIV were also the target signal. The main differentiator between the noisy whisker-induced WIVs and the signal WIVs was the frequency of the sensors' vibrations, any overlap of which limited how aggressively the noisy WIV could be filtered out.

1.2 Time Domain Analysis

The studies herein all primarily focus on the time domain, and all the various arrays and sensor designs discussed, function via the examination of when and how their signal output changes in time. The study builds upon two existing techniques for signal analysis focused on the temporal component. The first is Generalised Cross-Correlation (GCC) which is an established foundation for a lot of work on signal analysis, and so its application to this study will be described briefly. The second is an application specific adaptation of Pseudo-Range Multilateration, which itself is a major expansion on the idea of triangulation. The challenges and adaptations made to this method are therefore outlined below.

1.2.1 Generalised Cross-Correlation

Generalised Cross-Correlation (GCC) is one of several correlation methods that maps the degree of similarity between two signals. This method can additionally be used to identify a time shift at which the signals match most closely, by shifting the signal comparison at small time intervals, and finding the time shift at which the signals are most similar.

In this case, the time shift represents the time taken for the flow disturbance to move from the first sensor to the second. Every possible pair of sensors is evaluated, to build the Time Difference Of Arrival (TDOA) matrix for the next step. Not every pair of sensors can be meaningfully evaluated (due to noise, due to some sensors having not been disturbed by the flow, or having only been hit by the side of the vortex and therefore displaying an 'unusual' signal output). These poor correlations were identified, and filtered out, algorithmically.

CC was the most computationally expensive step of the calculations due to the desirably large number of sensors to be correlated. To minimise wasted computation time, measures were taken to identify the sensors outputting the clearest signal and the array was evaluated based on their signal output. Additionally, the size of the correlation window was reduced wherever possible, by examining the duration of the incoming pulses. Despite the computation costs, the reliability of GCC in noisy environments made this an indispensable step.

This 'simpler' method of CC was used instead of other methods (ROTH or SCOT) as it is reported to be more reliable in reverberant environments, and would possibly minimise the effects of any vibrations in the water tunnel and WIVs.

1.2.2 Pseudo-Range Multilateration

Traditional Pseudo-Range Multilateration (PRM) calculates the time and position of the source of an emitted sound or electro-magnetic (EM) signal. PRM relies on the known position of multiple receivers, a known, fixed, propagation speed of the signal, and/or a known time of signal emission, to estimate the distance to the emission source, and the signal's time of flight(ToF). Once the TDOA (Time Delay of Arrival) matrix has been found, there are several common methods(Fang 1990, Krause 1987, Geyer & Daskalakis 1998) for solving for the point of origin in 2 or 3 dimensions.

For applications seeking to capture hydrodynamic signals, only the position of the receivers (the sensors) are fixed, and thus the unknown speed of the emitted signal must be overcome without knowledge of the time of emission. This represents a significant departure from traditional methods that focus heavily on EM or acoustic signals. Where traditional multilateration calculates the point of emission from the intersection of the pseudo-ranges generated from the TDOA matrix of multiple receivers, here the angle of arrival of the source, and thus the propagation speed of the source, must be found first.

While it would be possible to limit the scope of observation to a narrow range of signal speeds that are of particular interest, this would be a very poor approach to the problem as this would impose great limitations on the potential applications of any such sensor. Further, anything but a very narrow band of signal speeds would incur a large degree of uncertainty within the proposed solver, and even a small degree of uncertainty in the signal propagation speed could cause considerable error in the localisation of a signals' source.

Therefore, a variation on traditional methods is proposed herein that takes the typical dimension scaling a stage further. For multilateration, one requires at least 'm' measurements, or 'receivers', for $m-1$ dimensions, usually 2 or 3, for planar or 'real world' environments. Here the multilateration algorithm is modified to operate on a basis of sensor triplets instead of pairs. This provides another measurement to offset the additional unknown. However, this requires significant modification of the typical multilateration solver as will be discussed later.

1.3 Motivation for research

Any object moving through a fluid produces coherent hydrodynamic signals, often in the form of vortex rings or shed vortical rollers. If these signals can be detected and correctly interpreted, various characteristics of the object can be identified. The frequency, velocity, size, shape, and orientation of shed vortices can tell us about the size, speed, bearing, direction of travel, and type of object that produced them. There are many barriers that must be overcome before we can realise this capability. In this thesis the focus is on improving the reliability and versatility of bio-inspired whisker sensors, that via a time domain based approach, can be used to capture the velocity, frequency, and orientation of shed vortices. The study also seeks to identify areas to improve the performance and readiness of the technology for deployment, investigating the impact of factors such as the size, spacing, and layout of the whisker array, as well as exploring alternate sensor materials and concepts that offer greater deployment versatility.

This project begins with observations from biological studies on the behaviour and whiskers of the seal. These studies have shown the remarkable tracking capabilities of the seal, as it makes use of the hydrodynamic trails of its prey to locate and catch small fish that have passed the seal's location over half a minute prior. There has been much discussion, as well as ongoing research, aimed at answering the question of which hydrodynamic signal the animal relies on when using its whiskers. Seals have been observed to protract their whiskers forward when hunting for prey. This can be attributed to the seal spreading out the whiskers to 'feel' a larger area, or moving the whiskers out of the seal's bow wake. Seals hunting in nature have been observed 'whisking' their whiskers whilst tracking prey and comparisons have been drawn with the whisking motion used by small mammals to detect texture.

Both biological, and many recent biologically inspired engineering projects have focused on the mechanism of whisker deflection to explain the animals' ability to track its prey. By far the most common approach is to use the magnitude of the whiskers' deflection, and the associated strain, either on the vibrissal tissue of the animal, or on the artificial whisker's strain gauge mechanism. Focusing on this mechanism provides the most information on the flow possible for a single whisker, allowing for flow speed measurement, and some attempts at direction of travel measurements.

The underlying problem with this approach is that with a single sensor it is significantly harder to extract sufficient information from the flow, in order to solve for the large number of unknowns, and to therefore build a complete understanding of the flow disturbance's passage. Secondly, the strain gauge must be calibrated at each flow speed, and any change in the whisker's mechanical properties due to material fatigue or temperature changes could lead to significant errors, with the same holding true for any changes in the fluid properties (due to temperature, multi-phase flows, or mixing of dissimilar fluids).

Finally, even those that have looked to arrays of whiskers focused on the bending magnitude with the goal of ascertaining the angle of arrival of a disturbance, have struggled as this relies on the approach of comparing the left and right side whiskers and seeing which are most disturbed. In many cases this produces reasonable accuracy in a left vs right side comparison but since it has been shown that seals can correctly distinguish contralateral impacts (signals originating on one side of the head that impact the whiskers on the other side of the head) the animals must be using more information than such a system can provide, as a simple left vs right comparison would not predict such a path.

This thesis does not seek to undermine these approaches, but rather takes further inspiration from nature to explore the function and advantages of utilising the time domain in an array of sensors to solve a system comprised of many unknowns, with the goal of tracking hydrodynamic disturbances of unknown characteristics.

The first area of research therefore addresses the correlation of time tracked displacement. The seal likely senses the order in which the whiskers are disturbed, and has an awareness of the rough time delay between whiskers. We anticipate that this could be the critical mechanism behind the tracking of hydrodynamic disturbances. We look to study this with high-speed imaging of an artificial seal head model with plastic whiskers.

The second area of research is focused on expanding the basic correlation principle into a method for tracking the bearing of a disturbance. Seals have been observed to reliably track a disturbance path even 30 seconds after the source has passed (Schulte-Pelkum et al. 2007), using two distinct modes. The first is a direct path that speaks to a clear read on the travel path. The second is an undulating pattern where the seal crosses the path repeatedly. The authors suggest that this pattern might allow a seal to relocate a lost or weaker trail, which suggests that the seal can follow a travel path even without precise direction. The study aims to achieve an accuracy level similar or better than that displayed by seals in live trials.

Further than this, the study hopes to produce sensors that can reliably detect the much stronger effects of both the prop-wash and ship wake of larger ships, at much greater distances, the former of which has been shown to be measurable from over 100m away (Liao et al. 2015) using an in-situ PIV rig.

The third area of research is aimed at developing a deployable system of whiskers that can be used to reliably track a disturbance source in an uncontrolled environment. This stage of research focuses on addressing the issues surrounding deployment of an artificial system of whiskers in such an environment, delving into a new fibre optic whisker sensor design and its many benefits, optimisation of the array, and optimising the computation of the data from the sensors for faster operation.

1.4 Thesis Structure

This thesis follows the prospective publication format in which three journal papers, following a cohesive theme, are combined to present a holistic picture of the research I have undertaken. Each of chapters 2-4 is dedicated to one of these papers and is structured as follows: Abstract, Introduction and Literature Review, Materials and Methods, Results, Discussion and Conclusions, and lastly a Critical Analysis section. This includes discussion on the study in context of other work, key takeaways, and further study or results that were undertaken as a result of general questions from reviewers. Chapter 5 contains overall conclusions, suggestions for further work, and finally, a progress report of my PhD period. The publications are listed below in the order of presentation, along with a few key points pertaining to each study.

Publications

1. Glick, R., Muthuramalingam, M., and Brücker, C. 'Fluid-Structure Interaction of Flexible Whisker-Type Beams and Its Implications for Flow Sensing by Pair-Wise Correlation', Fluids 2021, 6, 102 (2021).

    - A common school of thought on whisker sensors is that the bending magnitude (or displacement) is the critical measurement for understanding the fluid motion around a whisker.
    - This study demonstrated the potential for tracking fluid motion using the time domain by showing the highly correlated motion of pairs of whiskers.
    - We demonstrated that we could accurately calculate the travel velocity of a disturbance across two sensors using the time shift of this highly correlated relationship by using CC.
    - We demonstrated that this could be done consistently in noisy, turbulent, environments. Further, by adding synthesised noise we concluded that this could still be done reliably, even in a highly noisy environment with an SNR as low as 2.6.

2. Glick, R., Muthuramalingam, M. and Brücker, C. 'Sea lions could use multilateration localization for object tracking as tested with bio-inspired whisker arrays' Sci Rep 12, 11764 (2022).

- This study built on the findings of the first paper, and showed that an array of sensors, focusing on the time domain, can be used to track a passing disturbance in a way that all single sensor systems fail.
- A method for tracking the path of a disturbance using an array of sensors is presented, adapted from techniques used in acoustic source localisation, and navigational tools such as GPS.
- In addition to correctly assessing the travel velocity as before, we demonstrated that this model could calculate, with reasonable accuracy, the direction of arrival of a disturbance.
- This method sets itself apart from previous work on whisker sensors as the signal is treated as a complete unknown. Therefore, despite knowing nothing about the disturbance's characteristics, i.e. size, shape, energy, or velocity, the time delays across the array can be used to find a disturbance's speed and direction.

3. Glick, R., Fabian, M., Brücker, C., and K.T.V. Grattan. 'Tracking hydrodynamic disturbances with fibre-optic whiskers' Opt Lasers Eng (2023)

    - This study addresses some of the problems that separate a technique possible in a lab from a technology that can be deployed in the field.
    - A new glass-fibre whisker sensor is developed, which would enable the sensors to be deployed and monitored remotely with much greater ease.
    - We demonstrate that the performance of the new sensors is comparable to that of the previous sensors by looking at the SNR, and the subsequent DoA calculation accuracy.
    - We assess methods of improving the performance of the array using alternative sensor layout, spacing, and noise reduction techniques.
    - We conclude that deliberately irregular spiral arrays offer large performance improvements, that shorter inter spacing of the sensors can be beneficial despite the potential effects of WIV, and that the robust nature of CC means that computationally expensive noise reduction techniques are likely unnecessary for real time monitoring applications.

Chapter 2

Fluid-structure interaction of flexible whisker-type beams and its implications for flow sensing by pair-wise Correlation

2.1 Abstract

Background: Sensing of critical events or flow signatures in nature often presents itself as a coupled interaction between a fluid and arrays of slender flexible beams, such a wind-hairs or whiskers. It is hypothesized that important information is gained in highly noisy environments by the inter-correlation within the array. Methods: The present study uses a model sea lion head with artificial whiskers in the form of slender beams (optical fibres), which are subjected to a mean flow with overlaid turbulent structures generated in the wake of a cylinder. Motion tracking of the array of fibres is used to analyse the correlation of the bending deformations of pairs of fibres. Results: Cross-correlation of the bending signal from tandem pairs of whiskers proves that the detection of vortices and their passage along the animal's head is possible even in noisy environments. The underlying pattern, during passage of a vortex core, is a jerk-like response of the whiskers, which can be found at later arrival-times in similar form in the downstream whisker's response. Conclusion: Coherent vortical structures can be detected from cross-correlation of pairs of cantilever-beam like sensors even in highly turbulent flows. Such vortices

carry important information within the environment, e.g. the underlying convection velocity. More importantly in nature, these vortices are characteristic elementary signals left by prey and predators. The present work can help to further develop flow, or critical event, sensory systems which can overcome high noise levels due to the proposed correlation principle.

2.2 Nomenclature

Γ	Vortex Circulation Strength
CC	Cross Correlation
CFD	Computational Fluid Mechanics
DPIV	Digital Particle Image Velocimetry
FSI	Fluid Structure Interaction
IW	Interrogation Window
LES	Large Eddy Simulation
SNR	signal to Noise Ratio
PIV	Particle Image velocimetry
R	Vortex Core Radius
$\mathrm{Re}_{\mathrm{cyl}}$	Re-number based on cylinder diameter
Re_{d}	Re-number based on whisker diameter
U_∞	Free-stream Velocity
x_0	Undisturbed Whisker Position

2.3 Introduction

Fluid-structure interactions of flexible cantilevered cylinders have been studied for a long time (Bearman 1984). Most of the applications addressed in these studies were related to high-Reynolds-number flows in oil risers or heat converters, to name a few. Interest also arose in the flow around filamentous structures with submillimetre diameter, which are often found in nature in various forms. They function as antennae or sensing structures in animals such as in bats, cockroaches, or spiders (Barth et al. 2003). Furthermore, they appear as whiskers in pinnipeds, or seals, which live in the aquatic environment. The typical Reynolds-number of flows around those whisker-type structures is in the range between 10-1000 with Re_{d} based on the characteristic diameter of the whisker diameter d. As a typical feature, these sensing elements don't appear as a single structure but are instead arranged in arrays. The signal output is expected to be largely influenced by the arrangement of sensory hairs, as investigated in (Brücker & Rist 2014). This may allow the distinction of complex patterns from their spatio-temporal signature. It seems probable that this is important in nature, where the multi-signal sensor output needs to be selective enough to trigger specific tasks such as flow control or escape behaviour, under the influence of turbulent background noise. The first studies into neurological relevance of the cross-correlation of the signals of neighbouring sensory hairs in the aquatic world, have been investigated on the lateral line system of fish (Chagnaud et al. 2008). The spike trains taken from the primary afferent nerve fibres of a pair of neuromasts along the fish' lateral line system were cross-correlated, and the results provided the gross velocity of the fluid around the body of the fish. Therefore, the natural turbulent fluctuations in the water already transport the necessary information to retrieve the locomotive or convection speed of external flow patterns. The correlation hypothesis was also proven to work in engineering applications by using a pair of micro-pillar wall-shear sensors in a turbulent boundary layer flow (Chagnaud et al. 2008), where the same cross-correlation was applied to recover the convection speed of the external flow around the plate.

Further advancements in sensory applications were found in tandem pairs of cylinders mimicking sensory hairs, regarding their side-by-side arrangement (Axtmann et al. 2016). It was shown that the first cylinder can act as a flow preconditioner, serving to either improve the streamwise sensory response of the second sensor, or to shield it from streamwise fluctuations, while crossflow fluctuations remain unaffected. This would allow the system to be effective in sensing strong transverse motion patterns. Other aquatic species with slender cylinder-like sensors are sea lions and other pinnipeds, which can track their prey by using their whiskers as hydrodynamic sensors (Dehnhardt et al. 1998). Recent studies on fluid-structure interaction of artificial whiskers showed that the most important pattern of the dynamic response signal does not come from the flow fluctuations, but from the pressure distribution in a vortex that passes the whiskers (Muthuramalingam & Brücker 2019). The authors constructed a model sea-lion head, with optical fibres acting as whiskers, to better understand how the animal's whiskers responded to stimulation. By mimicking the wake of prey or predators, in the form of von-Karman type vortex streets, they found that the whiskers moved with each passing vortex in a jerk like manner. A distinctive "stick-slip" response pattern developed as a response to the pressure gradient in the vortex core (Muthuramalingam & Brücker 2019). This study showed, for the first time, that long whisker-type hairs are able to detect the passage of vortices, and that therefore, these sensors can be understood as "vortex detectors". This was a paradigm shift in the understanding of the whisker's response. Previous behavioural studies in controlled environments have shown that Harbor seals can sense the wake of prey over 30 seconds after the prey has past (Wieskotten et al. 2010). Our hypothesis is that weak signals like these can be better detected from a pair of neighbouring whiskers using their cross correlation, than from the bending signal of a single whisker alone. This could allow pinnipeds to distinguish a coherent signal from noise. (Estebanez et al. 2012) studied the neural response of rats to correlated whisker stimulation. They demonstrated that very few neurons responded to simple stimulation of a single whisker, but the neural response was far greater when correlated stimuli were introduced across multiple whiskers.

The goal of this study is to demonstrate that the pair-wise correlation of the whiskers' response can be used to detect coherent flow structures (vortices) passing the whiskers even in highly turbulent conditions, or at a very weak signal-to-noise ratio. This information is important firstly to detect typical vortex patterns left in the wake of prey or predators, and secondly to determine their velocity and convection direction relative to the swimming body. This could be an additional step forward in understanding the potential of such processing methods for target tracking. Our previous study, as a first step into using neural networks and deep learning

(Elshalakani et al. 2020), neglected the temporal pattern of the fluctuations and their coherence over the array of the fibres. Instead, it used only the RMS values of the fluctuation amplitudes as input from all the different fibres. Nevertheless, this trained model is already able to predict the near-by upstream locations of the cylinder to within 1cm accuracy (Elshalakani et al. 2020) . The present study is a continuation of our previous work towards a more sophisticated model, which will also include the temporal information of the sensors. CFD simulations and experimental studies of the flow around a model of a seal head, are combined to determine the response of arrays of whiskers to turbulent incoming flow. The disturbance in the flow is produced by a cylinder upstream of the seal, which generated a von-Karman vortex street. The vortices passing the whiskers generated fluctuating bending motions, which were recorded simultaneously for all whiskers and processed using cross-correlation algorithms. Finally, gross flow velocity is estimated from those correlations and compared to the predictions from CFD.

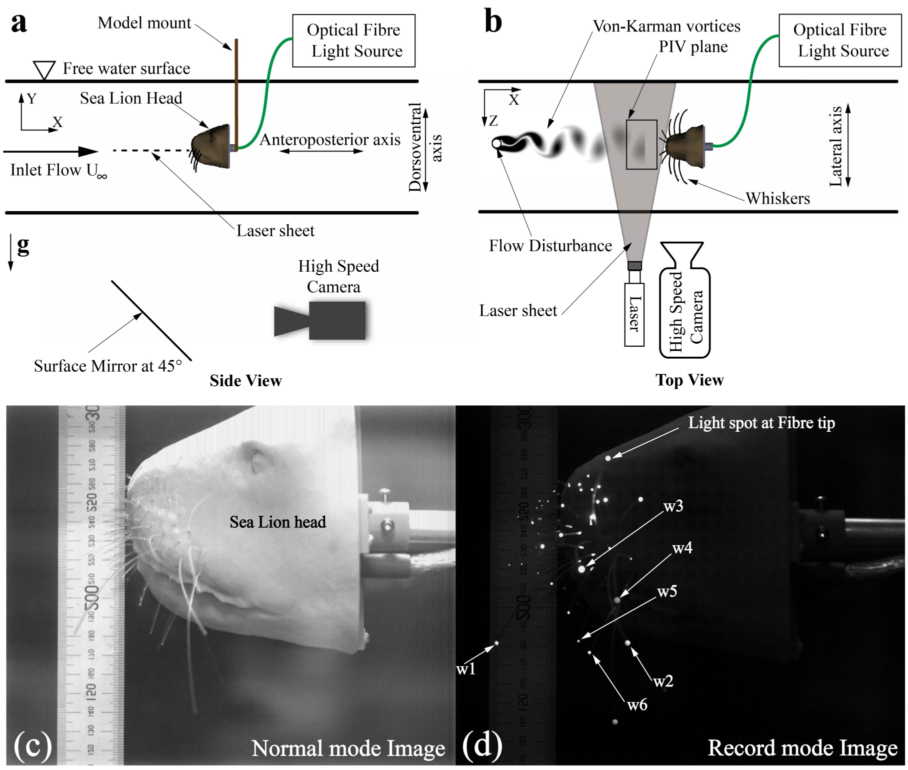

Figure 2.1: Schematic diagram of the experimental set-up, modified after (Muthuramalingam & Brücker 2019). (a) Side-view (b) Top-view. Von-Karman vortex street is shown for representation. (c) Normal mode photograph of the model from the camera (Scale in mm). (d) Image from the camera with reduced light and fibre optic light switched ON (the tips of fibres are visible as light spot) Note that the whisker numbering is used in the discussion of results.

2.4 Materials and Methods

2.4.1 Sea lion model with whiskers

The experimental model is the same as described in our previous work (Muthuramalingam & Brücker 2019) and the key features are described herein again. We use a 1:1 scaled model of the head of a sea lion with artificial whiskers (optical fibres, diameter $d = 0.75$mm), with a similar length scale, and at similar positions to the biological example. In addition, the material of the fibres has an elastic modulus, and diameter, similar to the natural whiskers (Muthuramalingam & Brücker 2019). The array of optical fibres are inserted through holes from the backside of the 3D printed model and are illuminated from one end such that the tips of the free fibre ends appear as bright spots, on both sides of the head. The fibres therefore represent one-sided clamped flexible cantilever beams with circular cross-section, interacting with the flow.

2.4.2 Experimental setup for motion tracking

The experimental setup is the same as described in our previous work (Muthuramalingam & Brücker 2019), except for the differences in experimental procedure and data processing. The sea lion model with its artificial whiskers, is mounted inside the measurement chamber of a return type open surface water tunnel with a velocity range of 0.1 to 2 m/sec. Flow straighteners were installed in the settling chamber, situated before the convergent section, to achieve uniform flow in the test section. The test section is 40 cm wide x 50 cm depth x 120 cm in length and transparent on all sides to provide optical access for flow studies. The model was placed at the centre of the test section, 70 cm down stream from the inlet as shown in fig. 2.1, and a wake generating cylinder was placed upstream of the sea lion model to generate turbulent vortical flow features that would pass the head and whiskers. The experiments were conducted with a cylinder of diameter $D = 30$mm at three flow velocities U_∞ of 20, 25 and 30 cm/sec. These parameters were selected based on findings by (Miersch et al. 2011). A high-speed camera (ProcImage 500-Eagle high-speed camera) at a sampling rate of 250 Hz was used to track the motion of the whiskers on one side of the sea lion model, as shown in fig. 2.1b. It had a pixel size of 1280 x 1024 which relates to a physical dimension of 238 x 190 mm. The built-in function in the camera calculates the tip coordinates in the (x, y) coordinate system of each light spot automatically using the barycentre mode. The measured signals are the tip deflections of each of the optical fibres captured simultaneously, which is directly proportional to the applied bending moment at the shaft of the whiskers (Euler–Bernoulli beam theory). For further details see (Muthuramalingam & Brücker 2019), and (Elshalakani et al. 2020).

2.4.3 Flow studies using PIV and CFD

A combined experimental and numerical study using Particle image velocimetry (PIV) and CFD was done to characterize the flow conditions in front and around the sea lion head. For PIV, a 2 mm thick laser light sheet was focused on the region upstream of the snout region of the sea lion head. The PIV images had a pixel size of 1280 x 800 with a physical dimension of 152 x 95 mm. Neutrally buoyant particles of 50 microns were seeded in the water tunnel, and were recirculated within the tunnel until the right amount of particles required for the PIV were observed. The images were captured with a Phantom Miro M310 camera using a 45 degree slant mirror as shown in fig. 2.1a at a frame rate of 250 Hz and for a flow time of 4 seconds. Classical digital cross-correlation (DPIV) is used to obtain the 2D velocity vector field in the plane, using an iterative interrogation window (IW) refinement procedure (starting from 64x64 IW size) and sub-pixel accuracy analysis from a Gaussian fit to the correlation peak.

Figure 2.2 shows the computational domain used in LES simulations. The domain extends 400mm in Y and Z directions and 1200mm in X direction, which is comparable to the experiments. The outer faces are discretised with 2mm structured hexahedral elements and the cylinder circumference is discretised with 400 mesh points. The first cell distance from the cylinder surface was 0.04 mm which resulted in a y+ value less than 1. The domain around the sea lion head was meshed with unstructured tetrahedral elements which resulted in a total mesh size of 9.2 million. The Large Eddy Simulation was performed with commercial CFD solver: Ansys Fluent, version 19.0 using WALE (Wall-Adapting Local Eddy-viscosity) subgrid scale model (ANSYS 2019).

In a first approximation, no whiskers were considered in the mesh, as the key information on the FSI necessary for testing the correlation hypothesis has already been obtained in high quality from prior detailed experiments (Muthuramalingam

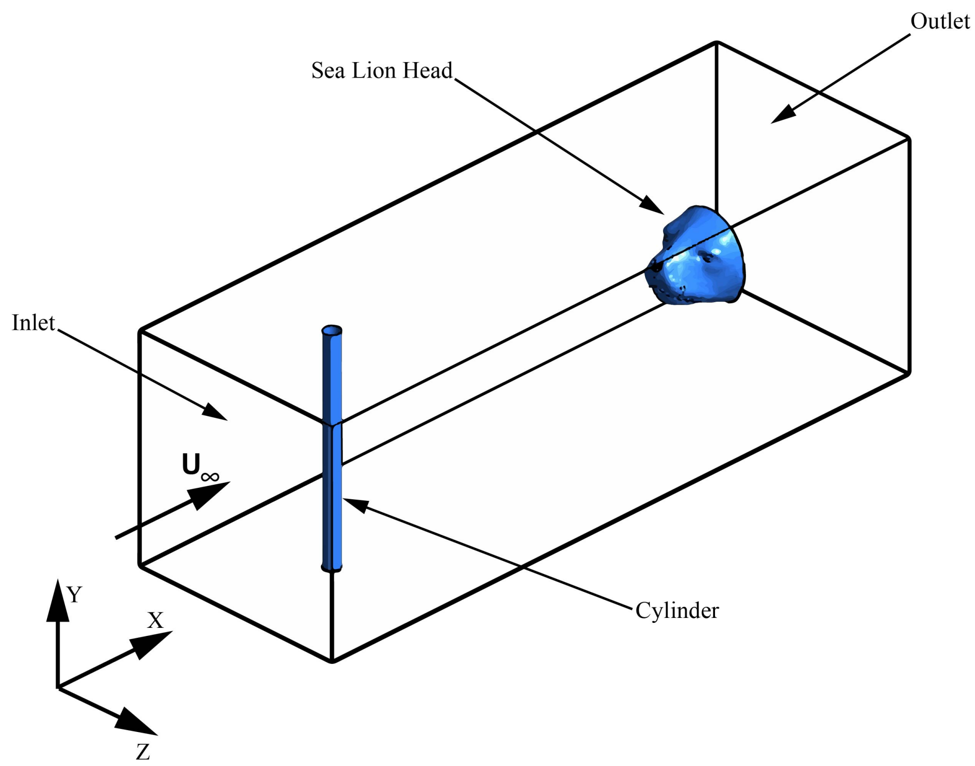

Figure 2.2: Sketch of the CFD domain and the flow configuration similar to the experiment. The domain extends 0.4m in Y and Z directions and 1.2m in X direction.

& Brücker 2019). The complementary CFD simulations are mainly utilised to determine the global flow field around the head, which is difficult to achieve otherwise. It is difficult to determine from a PIV experiment because of the whiskers obstructing the optical view in the light-sheet plane close to the surface of the model. Furthermore, a fully two-way coupled FSI simulation of the current 3D problem requires an immense amount of computing effort; it would require solving the FSI at all required spatial and temporal scales, whilst fully resolving the dynamics of all whiskers along the model seal head. As the diameter of the whiskers is more than two orders of magnitude smaller than the characteristic scale of the head, very small time-steps on a very large mesh need to be considered for physical time periods of minutes. This illustrates the dilemma of such simulations and explains our approach of combining CFD (without the whiskers) and experimental data (with whiskers) with exactly the same boundary conditions. Note that we assume in this first approximation that the gross flow around the head is not affected by the presence of the tiny whiskers. The inlet was specified with constant velocity of 30 cm/sec with inlet turbulence value of 0.3%. The momentum equations are discretised with central differencing and second order scheme was used in time discretisation with a time step value of

0.004 seconds which relates to 120 time steps per shedding cycle calculated from the Strouhal frequency.

2.5 Results

Figure 2.3 shows an instantaneous flow pattern of the cylinder wake when the cylinder is placed ahead of the snout of the model along the body axis. The underlying disturbances in the flow field are produced by the von Karman vortex street, generated in the wake of the upstream cylinder, producing a periodic shedding of coherent vortices (quasi 2D vortex rollers, with their axes aligned with the cylinder axis). The Reynolds-number, defined with the free-stream velocity and the diameter D of the cylinder, is $\mathrm{Re}_{\mathrm{cyl}} = 9000$, which is clearly in the turbulent wake regime. The shedding pattern in the horizontal plane (crossing the model axis) is similar to that of the so-called "inverse" von Karman vortex street, which is found in the wake of swimming fish due to the periodic body and fin undulation (Müller et al. 1997). The direction of rotation of the vortices in the fish wake is the inverse of that which is found in the cylinder wake, however the pressure distribution in the vortices is similar (Videler et al. 1999). For comparison, fig. 2.3 also illustrates the time-averaged flow pattern. From that we see the typical velocity deficit in the wake of the cylinder and the "bow wake" effect in front of the snout (due to the effect of the displacement body). As a consequence, short whiskers around the front part of the snout "feel" the flow disturbances passing by with lower velocity than long whiskers at the more lateral side of the snout, which stand out of the bow wake region in the free stream.

The velocity field results from LES were compared against the PIV measurements in the region upstream of the snout, both show a similar decrease of the streamwise velocity near the snout, see fig. 2.4. Note, that the bow-wake effect has been shown to play a large role in hunting and predator escape as documented in (Kogan et al. 2015).

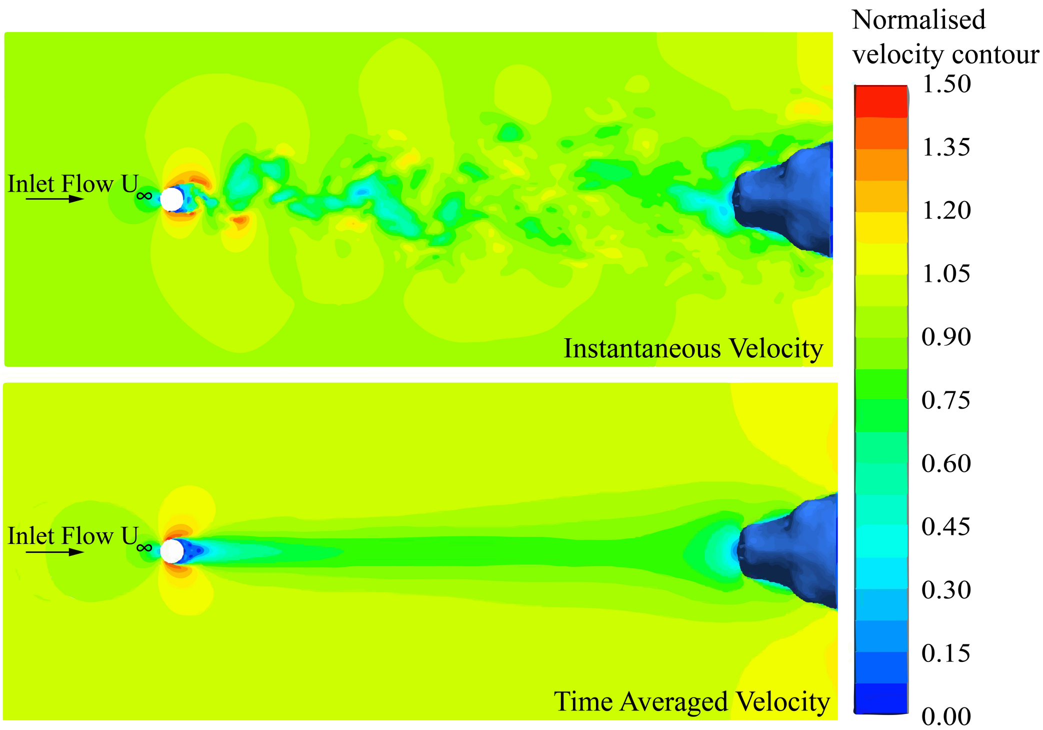

Figure 2.3: Velocity field through the test section from CFD Simulation (displayed as colour-coded contours of constant streamwise velocity). Top: Instantaneous velocity field, Bottom: Time-averaged flow pattern.

2.5.1 Typical whisker response

In the following sections, the results are presented for both short and longer whiskers (50mm and 100mm, respectively), the short ones being tested with the cylinder placed along the body axis, while for the long ones the cylinder was moved transversely to a distance of 100mm away from the axis. This is to ensure that the vortices pass along the tips of the whiskers in all experiments. Note that the major component of the bending motion is in streamwise direction, parallel to the dominant fluctuations in the velocity field of the shed vortex rollers. We have taken a 3-4 minute recording for each of the inlet velocities U_{inf} = 20, 25, and 30cm/s . Our analysis data set size is typically a time-window of around 40s, therefore for each experiment we have 5-6 independent samples. An example of a short sequence of individual whisker responses to the passing of von Karman vortices is given in fig. 2.5, shown for whiskers w1 & w2 with a freestream velocity U_{inf} at 25 & 30cm/s. The plot shows the time-dependent tip location of the bending beams (in streamwise direction) with the mean removed. With a typical Strouhal number of roughly 0.2 for cylinder wake flows (Blevins 1990) we expect the shedding frequency at 30cm/s

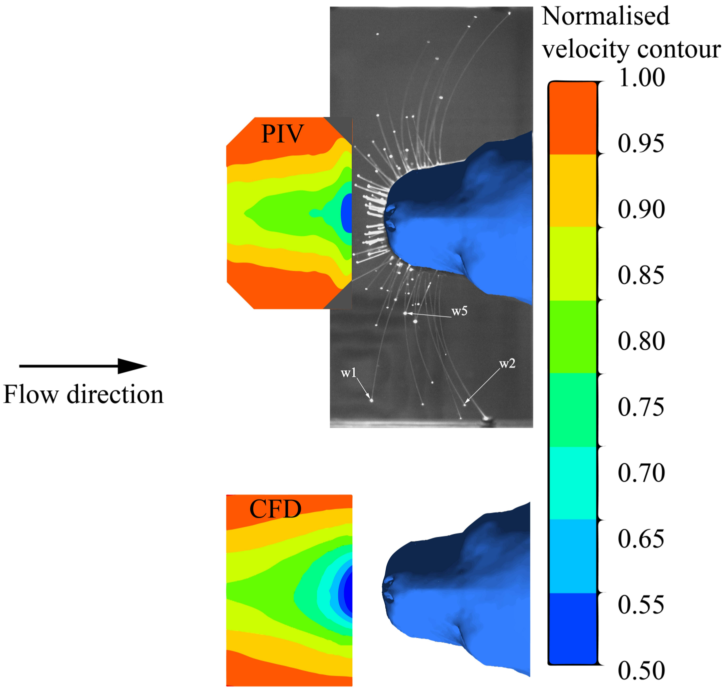

Figure 2.4: Bow-wake region in front of the snout from experimental flow field measurement using PIV compared to the CFD flow field (displayed as color-coded contours of constant streamwise velocity).

to be 2Hz (for cylinder diameter of D=30mm), which should correlate with the periodicity of the whisker's motion. As can be seen in Figure 2.5 the tip motion of whisker w1 exemplifies the expected periodic character of the deflections, overlaid with random fluctuations due to the turbulent nature of the flow. For comparison, the tip-motion of whisker w2 is overlaid on the same plot, which is positioned in the roughly the same horizontal plane further downstream of whisker w1 and has the same length as w1. It is obvious from the time-patterns that the response is similar, albeit shifted in time. This calls for the investigation of the pair-wise correlation hypothesis given above.

2.5.2 Pair-wise correlation of whisker motion

The characteristic jerk-type response of the whiskers during passage of a vortex is the signal that provides the largest contribution to the correlation peak, while random motion does not correlate. To test this hypothesis, the temporal traces of the whiskers' tip-motion were cross-correlated (time-window of 40s) and the time-lag at the peak location was considered to represent the corresponding average travel time of the vortices between the tip-locations. The estimated convection velocity values between the pair of whiskers w1 & w2 are given in table 2.1, in addition to the

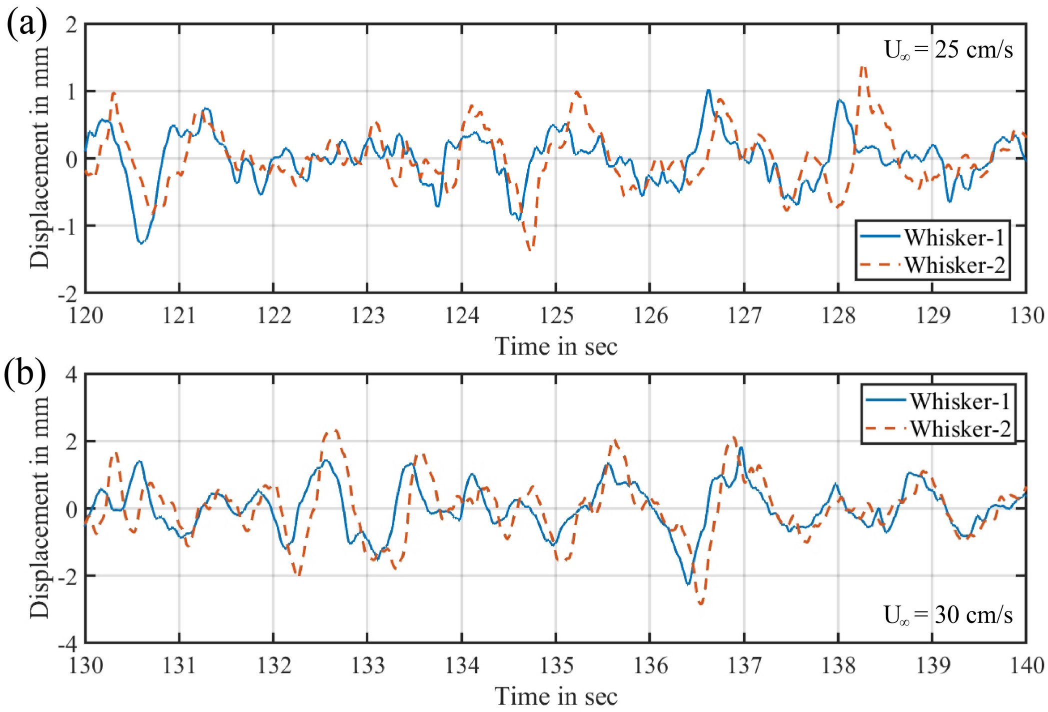

Figure 2.5: Fluctuating tip-motion of a pair of whiskers w1 & w2 in the wake of the cylinder (a): freestream velocity $U_\infty = 25$cm/s, (b): freestream velocity $U_\infty = 30$cm/s. The time-traces show a series of similar characteristic jerk motions, off-set from each other by the time taken for vortices to travel the distance between the whiskers (mean component subtracted).

free stream velocity, and the local velocity at the location of whisker w2, taken from the LES results of the flow field around the head. As both whisker w1 & w2 are long enough to extend outside the influence of the bow wake of the model (w1 and w2 as shown in Figure 2.1, both of length 100mm), the estimated convection velocities are close to the free-stream velocity. A slight overestimation is observed due to the body displacement effect, shown in fig. 2.3 by the accelerated flow around the sides of the head, where the whiskers w1 and w2 are located. The reference velocities shown in tables 2.1 & 2.2 are taken from the LES results at the whisker w2 location.

Another pair of whiskers were chosen for further testing the correlation hypothesis. This time, a pair with different lengths were selected (w1 and w5, the latter with 50mm half the length of w1). This was to investigate possible effects of structural instabilities of the whiskers on the CC results, as different beam lengths also means different characteristic frequencies of the bending modes under dynamic fluid loads. The calculated free stream velocity values from this pair-wise correlation in table 2.2 are notably lower than the actual free stream velocities since much of whisker w5's length is inside the bow wake region. Therefore the vortices are travelling at lower convection speeds across w5. This is also justified by the lower velocity reference

Table 2.1: Results of the measured convection velocity by cross correlation (CC) of whiskers w1 & w2, situated outside of the influence of the bow wake. Local reference velocity at position w2 is taken from the LES simulations in Figure 2.3.

U_∞ (cm/s)	Local velocity (cm/s)	CC Velocity (cm/s)
20	20.8	21.2
25	26.0	26.1
30	31.2	30.9

Table 2.2: Results of the measured convection velocity by CC of whiskers w1 & w5, the latter being situated inside of the influence of the bow wake. Local reference velocity at location w5 is taken from the LES simulations in Figure 2.3

U_∞ (cm/s)	Local velocity (cm/s)	CC Velocity (cm/s)
20	18.2	18.0
25	22.8	22.6
30	27.3	26.9

values at the whisker tip location, from the LES.

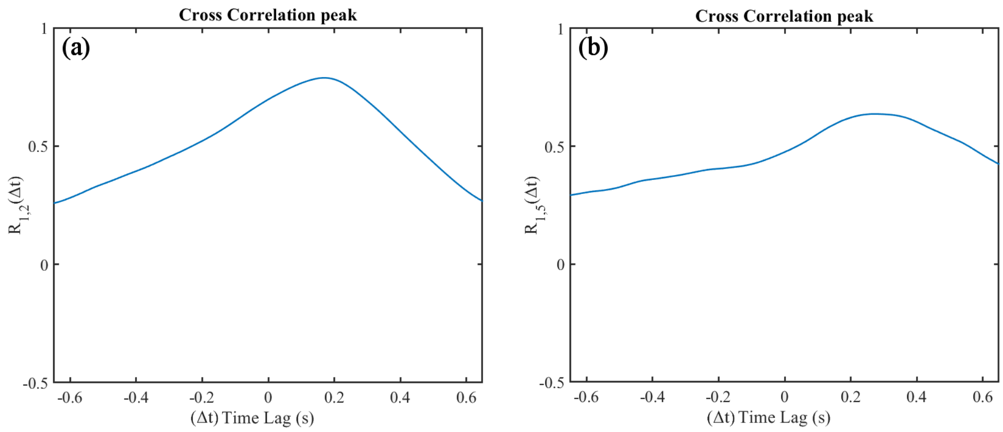

Figure 2.6: Typical profiles of the cross-correlation function around the peak for tunnel flow speed at 20cm/s. (a) CC of whiskers w1 & w2, peak value of 0.78. (b) CC of whiskers w1 & w5, peak value of 0.62. The greater time delay in B) is due to the lower velocity, as discussed above.

All correlations so far were done with a time-window of 40s, which is equivalent to the passage of about 80 shed vortices. Typical SNR values of the CC peak (ratio of the primary peak height to 2$^{\text{nd}}$ peak) were found to be 10 for all tested configurations. For steady background flows, even a shorter time window containing a jerk-signal of a single vortex may be strong enough for a reliable cross correlation. However, the turbulent nature of the wake flow at $\mathrm{Re}_{\mathrm{cyl}} = 9000$ herein requires a larger number of coherent structures passing by to keep such a high SNR of the CC peak. When the time window was shortened below 10 seconds, the quality of the CC peak diminished and random fluctuations caused shallow, split CC peaks, which could not be qualified as representative of the overall flow field. On the other hand, when the time window became too large, the CC peak became flattened due to the overall time-averaging effect of the turbulent flow. The above discussion pertaining to the influence of the number of events on the CC, only relates to a single whisker pair. It is obvious that a larger number of whiskers, given that there are typically 38 whiskers on each side of the sea lion, would greatly improve the SNR when using a global correlation. Seals may also detect single vortex structures in a turbulent environment by using a global correlation involving all their whiskers simultaneously.

2.5.3 Simulation of noise effects

For further investigation of the influence of background noise on the correlation signal we use the theoretically derived response of the beam for the passing of a vortex (see the mathematical derivation given in Appendix 1 in (Muthuramalingam & Brücker 2019)). The Gaussian pressure drop in the core of the vortex leads to a jerk-type response of the beam in form of the time-derivative of the Gaussian:

$$J(t) \propto \Gamma \frac{(U_\infty t - x_0)}{R} exp\left(\frac{-2(U_\infty t - x_0)^2}{R^2}\right) \tag{2.1}$$

where Γ is the circulation strength of the vortex, R is the radius of the vortex core and x_0 is the location of the leading whisker relative to the trailing whisker (position $x = 0$). At $t = 0$ the incoming vortex has hit w1 at $x = -x_0$ and travels further towards w2, where it hits with a time-lag of $\Delta t = x_0/U_\infty$, i.e. the time taken for the vortex to travel the distance between both whisker. This signal is used to investigate the cross-correlation with different levels of noise overlaid. Figure 2.7a, shows a generated jerk signal, with high levels of random background noise and its time-shifted counterpart, again with high level of noise. Despite this, without any filtering or smoothing, a strong correlation can still be seen in the expected region of time lag as shown in fig. 2.7b. However, the maximum position of the curve is not clearly visible as it was in the previous situation without noise. The random noise introduces uncertainty in the position of the true peak. As the base signal is of type of a Gaussian function, the peak region in the cross correlation profile can be approximated with a Gaussian function, too. This technique is known in Digital Particle Image Velocimetry as peak fitting and allows one to achieve sub-pixel resolution (Raffel et al. 2007). The same methodology it is used herein to fit the peak region, see fig. 2.7c. As a result, we have found that even for high noise levels, where the random noise is almost 50% of the amplitude of the signal, the fitted Gaussian curve produced the time lag with 95% confidence, to within$\pm$ 5.4% of the correct time lag.

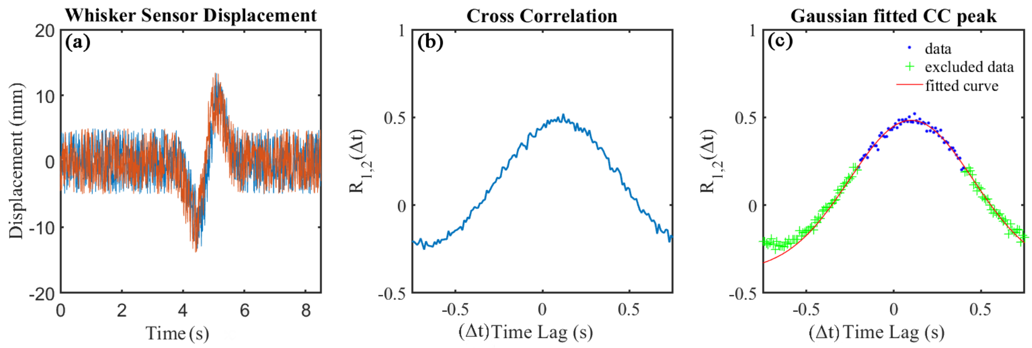

Figure 2.7: Synthetic jerk-pulse with added random noise and its CC profile. (a) jerk signal with an SNR of 2.6 in original (red) and time-shifted with 0.1s (blue), noise addition is random and independent in both signals. (b) CC of the noisy signals, showing erratic fluctuations near the peak. (c) Gaussian curve fit in the peak region with a clear maximum at the expected time-lag.

2.6 Discussion and Conclusions

Previous work by one of the authors and colleagues (Chagnaud et al. 2008) describes the lateral line system of fish, and how this system can determine gross flow direction and velocity from cross-correlation of the signals from the neighbouring neuromasts. The present study aimed to test this hypothesis for application in whisker-type sensors.

The pair-wise correlation of flexible beam motion for sensory application in nature (and engineering), has been investigated herein for slender cantilever beams of sub-millimetre diameter, similar in shape, size and mechanical properties to those of sea lion whiskers (for detailed material parameters see our previous work (Muthuramalingam & Brücker 2019)). For such whiskers, paired with typical animal swimming speeds of order of 1m/s, the Reynolds-number of the local flow around the beam is still in the low to moderate Reynolds-number regime (Re_d ¡ 1000). When tested for their response to a von-Karman vortex street of an upstream located cylinder we found that each time a coherent vortex passes a beam, a jerk-type response of the beam is observed, which is caused by the force induced by the Gaussian pressure drop in the core of the vortex (see also the mathematical derivation given in the Appendix 1 in (Muthuramalingam & Brücker 2019)). This signal is an ideal candidate for estimating the convection velocity of these embedded structures via a pair-wise correlation of the bending of neighbouring beams. Indeed, the correlation signals show a high signal-to-noise ratio of about 10 (ratio between 1^{st} and 2^{nd} peak) and can clearly decode the convection velocity, in low-turbulence background flows even from a single vortex event. On the other hand, the strong correlation also provides a way to distinguish existing vortical structures from noise when such events hit the whiskers along the body of the animal. This allows the animal to sense characteristic hydrodynamic signals left by prey or predators in their wake. Additionally, this could also allow for further investigation into whether the sea lion, or other pinnipeds, utilise the combined signals from multiple whiskers, and if the time shift of hydrodynamic stimuli is a factor.

Engineering applications of pairs or arrays of whisker-type sensors can be envisioned in a similar way to detect hydrodynamic signals of wake-generating bodies or swimmers in aquatic environments, or to provide a robust way of sensing the swimming speed. On a smaller scale, flexible beams in the form of micro-pillars have already been used for measurements of the wall-shear stress signals in turbulent boundary layer flows in air and water (Brücker et al. 2005). Therein, the passage of strong events of sweeps or ejections could be detected in a similar way from cross-correlation as a kind of "event" detector. Further improvement of the accuracy of the time-lag is possible using a Gaussian fitting procedure of the correlation-peak. The beauty of such signal processing is that such events can be detected even under conditions of high-levels of noise (weak SNR). In addition, it does not require detailed calibration of the single sensors, it is only necessary to have a-priori knowledge of their dynamic response, see also (Brücker et al. 2007). Therefore, such data processing is superior to any processing of a single sensor.

The investigations herein are limited to thin slender beams with typical interspacing of more than 20 times the diameter d of the whiskers, similar to the widely distributed whiskers of the seal. These are therefore only minimally affected by galloping, which is often observed in tandem arrangements of larger cylinders (Bearman 1984). In addition, we have only tested the pair-wise correlation for whisker pairs placed in a similar horizontal plane of the head. Certainly, the more complex arrangement of the whiskers on a pinnipeds' head requires further study of these effects and possible applications to 3D flow disturbances. Future research will focus on furthering the usage of the correlation hypothesis for the detection of distance and direction of the source. In principle, the disturbances generated by the cylinder are periodic patterns, however our theoretical results with single jerk-signals show that the pair-wise correlation can also work based on single pulses or events, where single vortices hit the head. This is current work in our lab, which may also support behavioural studies on seals to detect the direction of incoming hydrodynamic disturbances (Krüger et al. 2018).

2.7 Critical Analysis

This paper is the basis on which much of our more recent research is built. We utilised flow simulations to predict the flow pattern around the experimental model, and verified the flow field using PIV. This was then compared with the flow speed estimations of the tracked whiskers on the experimental model, finding clear results that closely followed the CFD simulations and PIV measurements. This was further verified with a frequency analysis of the system. By comparing the theoretical shedding frequency of the shedder bar (1.75Hz at 25cm/s) to the oscillation pattern of the disturbed whiskers (roughly 1.7Hz), we could see with confidence that the system was correctly picking up the correct signal. We further consider the frequency of the whiskers' oscillation and see that this is also sufficiently far from the whiskers' natural frequencies (0.35, 3.2, and 6.5Hz), and WIV and VIV frequencies (70+ Hz). In theory the WIV frequency of the cylindrical whiskers can inform on the flow velocity but this is subject to much larger error margins and cannot be used by itself to investigate sudden fluctuations i.e. a flow event. Further confirmation of the unsuitability of frequency analysis in solving the presented problem, comes from a biological study on whisker frequency sensitivity (Murphy et al. 2015). The authors found that real whiskers are most sensitive to frequencies in the range of approximately 20-250 Hz. This matched the control of a human touching the vibrating source, indicating that whiskers are most sensitive to frequencies outside of the frequency range of hydrodynamic signals emitted by their prey.

General questions raised by reviewers

1. **The whiskers are omitted in the CFD model and as such an FSI simulation of the whiskers has not been performed. How can one be sure that the whiskers do not significantly affect the flow locally?**

   The primary factor that minimises the importance of modelling the whisker FSI is the diameter of the whiskers being more than two orders of magnitude smaller than the characteristic scale of the body of the head. Further, the whiskers are often vertically offset from each other and therefore the whisker would not influence those behind it. We therefore suggest that the gross flow around the head is not affected by the presence of the whiskers. Therefore, we simulate the flow next to the Sea lion in the absence of the whiskers to provide the local flow field around the head affected by the body displacement effect.

2. **How reliably can time delays be used to calculate velocity estimates if the path of the disturbance is unknown?**

   This study was conducted in a simple flow situation where we emulate an animal moving forwards. This means the vortices arrive from the front and move along the length of the model. Therefore two whiskers placed along the length of the animal can accurately measure the velocity of the flow. In an environment where the flow direction is unknown, so too would be the path of any disturbances. Using the current method, the sensors would only measure the axial component of the velocity, resulting in a significant under-estimation of the flow speed. Therefore, estimating the direction of a disturbance's travel is not only useful by itself, but would also enable more accurate estimations of the disturbance velocity. As such, this is a key objective that we will focus on in further studies.

3. **On a 3D model such as the one used in this study, the sensors fan out around the vibrissal pads, but only the tips are tracked. To what extent does uncertainty in the position of the impact site hinder the calculation of velocity or direction?**

   Although the whisker root and tip locations are known and tracked respectively, when dealing with small flow disturbances of diameter less than the length of the whisker, a vortex core could strike the whiskers at any point in between. If the calculation of the speed is based on the distance between the whisker tips then this could over or under estimate the flow speed based on the true distance between the whiskers' contact sites. When looking at the seal's vibrissal pads, it is clear that the whiskers are placed in a ordered fashion, and as such the distance between whiskers generally scales evenly from the root to the tip. The same is largely true for our model and by seeing which other whiskers are deflected it becomes clear roughly how far along the whisker the vortex impacts. By using a scaled blend of the tip and root distances, a more accurate distance between whiskers can be found for cases where the difference is great.

4. **Can the sensors operate reliably in a 3D flow, and if so how would**

one solve the issue of the unknown vortex path between the whiskers.

The axial component of a disturbance's velocity could be monitored via the coalescence or rarefaction of the whisker tips as utilised in (Bruecker 2016), and once the axial component of the flow disturbance is known, the sensors could add this component to their output. This performed very poorly for the seal head model used in this paper due to the irregular whisker layout, insufficient whiskers on the vibrissal pads, and the relative inflexibility of the mystacial whiskers. The revised layouts of subsequent whisker arrays to be used in future papers may function better with this method.

Recent studies relevant to the paper

In the time since this paper was published there have been several studies published that are relevant to this work.

A review of whisker inspired flow sensing mechanisms (Zheng et al. 2021), published shortly after the work above, highlighted the surprisingly broad range of approaches to whisker sensors. Despite the scope of the paper, there was a noticeable lack of studies covering the use of temporal analysis, or studies that considered the response of the whole array of whiskers to stimuli. The authors emphasised the need to further the understanding of how a whisker array can conduct multi-point velocity measurements within a hydrodynamic trail, and then interpret and process this information to deduce the size, shape, and direction of the disturbance source.

In the work above we demonstrated how a whisker array can conduct concurrent measurements of multiple velocities of different points within a flow field. This provided further confidence in the novelty and importance of our work, and left us confident that the approach employed therein could be expanded and refined to fully understand the mechanisms behind whisker flow sensing, allowing the deduction of the size, shape, and direction of a source.

Lie et al. (Liu et al. 2021) performed a numerical study looking at the correlation between fluid structures and the signals from a whisker array. They found that the strength, timing, and direction of the flow were the core properties affecting the patterns in the mechanical output signal of the whiskers. They found that the weakest flow disturbances produced the weakest mechanical signals, yet the whiskers could still pick up the patterns used to determine the timing and direction of the flow structures. It therefore follows that an whisker sensors based primarily on the time domain would be able to detect both weaker, and a wider range of flow structures than any system relying on the mechanical signals themselves. Although, the extent of this likely hinges on the ability of the system to capitalise on the noise reduction features observed in real whiskers.

Bodaghi et al. (Bodaghi et al. 2023) conducted an interpretable machine learning study via a numerical assessment of the fluid-structure interaction of whiskers and wake disturbances in the flow, isolating the flow structures that inform whisker sensor systems. Thus, enabling the identification of the most significant spatio-temporal signal patterns crucial for the network's predictions.

The study goes on to highlight the importance of temporal dynamics when interpreting the methodology of their machine-learning model, supporting the direction taken by our studies. Additionally, they note that as in our study above, they found that the longest whiskers positioned to capture the fastest areas of the flow, were the most important sensors for their predictions. This supports our later decision to simplify the whisker system by using only one size of longer sensors in the sensor arrays, despite the theorised ecological value (Grant & Goss 2022) of the shorter sensors to the seal.

Gong et al. (Gong et al. 2023) used a similar style of setup to ours to study the whisker's response to variations in the streamwise distance to the cylinder. The cylinder responsible for causing the flow disturbances was gradually moved away from the model. They found that for interactions beginning with the smallest distance that increased over time, the whiskers were more sensitive, but that at above a certain threshold the starting conditions made little difference to the signal output. they also noted that the whiskers could still detect the signal from the cylinder at over 240 cylinder diameters downstream. This highlights the remarkable capability of whisker sensors to isolate the signal from the noise of the flow, and their capability in detecting moving targets even with large streamwise gaps.

Chapter 3

Sea lions could use multilateration localization for object tracking as tested with bio-inspired whisker arrays

3.1 Abstract

Previous behavioural research on live sea lions has shown that they are able to detect the direction of oncoming vortices, even when impacting contralaterally. These experiments showed that the whisker system and the animal's neural processing is seemingly able to detect the Direction of Arrival (DoA) from just one side of the heads vibrissal pads. Therefore, temporal differences between whisker stimulation is a likely method for determining the angle. Herein, a theoretical model is presented based on multilateration, and tested by experimental studies on a 2D array of bio-inspired whiskers with regular spacing, and a 3D array of bio-inspired whiskers on a model head of a sea lion, as used in our previous studies. The results show that arrays of whiskers can in principle work as antennae to determine the DoA. This detection of the DoA is achieved by cross-correlation of triplets of whiskers, and Time Difference Of Arrival (TDOA) based multilateration, a method similar to signal processing in modern communication systems and other source localization applications. The results on the 2D array are conclusive and clearly support the hypothesis, while increased uncertainties were found for the 3D array, which could

be explained by structural shortcomings of the experimental model. Possible ways to improve the signal are discussed.

3.2 Introduction

The capability of sea lions to track prey-induced flow disturbances in the aquatic environment, even long after the source has passed the path of the seal lion, is still a fascinating subject of research. It shows the extraordinary sensitivity of the natural whiskers and the neural processing, which allows the sea lion to distinguish between different sources and the specific pattern left in their wake. Bio-inspired whisker sensing systems, with high sensitivity and selectivity, are highly useful to autonomous underwater vehicles, and would expand upon existing sensing capabilities in diverse aquatic environments. Increasing concern around the environmental impact of active sonar (Dolman et al. 2011, DeRuiter et al. 2013) make such systems unappealing for some applications, creating demand for alternative, more unobtrusive systems, that can detect a range of different signals. Artificial Whisker-like flow sensors are being tested with the goal of extracting information from the flow, either in form of vibrational response or bending response. On a small scale, micro-pillar sensor in form of small cantilever beams have been used to study near-wall flow features optically (Bruecker 2016). Other research groups have tested MEMS-based electronic stress sensors attached to the base of whisker like sensors for various applications, across a wide range of sizes (Deer & Pounds 2019, Zhang et al. 2021). Other recent technologies utilising similar sensing principles include patterned carbon nanotube and silver nano-particle composite films (Takei et al. 2014) which use the piezoelectric effect to map the stress at the base of cantilever beams. These systems provide a basis for further research on hypotheses of fluid-structure interaction of arrays of sensors, and to better understand the principles of multi-sensor signal processing in the neural system of the sea lion, something which can otherwise be difficult to gain from live seal experiments.

Detailed flow-structure interaction was mostly tested first on single artificial whiskers, where the source of flow disturbance was often imposed in form of a von-Karman vortex street, simulating the wake of fish and generated by placing a cylinder upstream of the whisker. This causes a disturbance pattern that contains quasi-periodic fluctuations, as produced by the passage of rows of vortices, produced by the perpetual shedding from the shedder body. Consequently, the focus of research was to investigate the adaptation of the sensing system to detect dominant frequencies within an otherwise unidirectional mean flow. As such, the hypothesis of Galloping adaptation (Mannini et al. 2014) evolved from such experiments. The results are based on an ideal situation when the hydrodynamic signal is a regular chain of closely staggered tubular vortex structures, aligned perpendicular to the planar whiskers. Another hypothesis, the jerk-type response adaptation, was developed based on similar studies with von Karman street type hydrodynamic disturbances using a sea lion head model, developed in our lab. Studies with arrays of artificial whiskers have shown that deep neural network systems are able to predict the location of the source of the von Karman wake (produced by a cylinder in the flow) in the near field with good accuracy in both distance and angle of the source relative to the snout (Elshalakani et al. 2020). Those measurements were based on the rms-values of the whisker tip fluctuations as a measure of the fluctuating bending stress at the root. Good predictability was achieved when the system was trained with the same source in repeated positions. Additionally, the wake passage was always parallel to the body axis. An open question remains as to how such a system will respond to single events that hit the whiskers from different directions or with different strengths. In nature, the hydrodynamic trail of an upstream swimming object could also consist of rather isolated vortex structures, such as for a burst and glide swimming style (Wieskotten et al. 2010). Therefore, the signal will not always be periodic and the flow disturbances could have both unknown speeds and directions of origin.

Recent animal studies from the University of Rostock, Germany (Krüger et al. 2018), have proven that the seal lion is reliably able to detect the direction of arrival of a single disturbance in form of a vortex ring, shot at the seal's head from some distance away. These results were obtained from behavioural studies of blindfolded stationary harbour seals, which were trained to respond to single vortex rings. The results show that harbour seals are able to correctly identify a variety of different vortex rings by turning their head towards the source, upon vibrissal stimulation. The authors speculated from their results, that a possible way that sea lions determine the direction of the vortices, is via the combined stimulation of the vibrissae of both vibrissal pads (left and right in the lateral plane) with a velocity difference. This would be comparable to the intensity difference in auditory localisation (Mills 1958). Indeed, the results obtained with the bio-inspired sea lion head model (Elshalakani et al. 2020) have shown, that for periodic excitation by vortices in a von-Karman wake, it is possible to detect the direction of the source just from the magnitude of the whiskers vortex-induced vibrations (VIV) when compared within the array. This hints to a mechanism which is sufficiently predictive just via left-right comparison of the intensity of excitation. However, one striking result of the Rostock's group studies was, that seals can also be trained to detect the travel direction with contralateral stimulation. This means that the vortex ring was passing only one single pad and without direct impact on the muzzle, see travel path 3 and 4 in Fig. 2, of their work (Krüger et al. 2018). This is the more natural situation when the seal lion encounters the wake of a swimming object with the whiskers protracted. The results showed that the animal was able to turn their head towards the direction of the source, on the opposite side to where the disturbance had been received. Therefore, it is important to further research the influence of temporal coding within the array on the response. Interesting in that context is the recent study (Glick et al. 2021) with pairs of artificial whisker proving that a pair-wise cross-correlation of whiskers can decode the convection velocity. These time delays can be further used to triangulate the position of the source, using techniques adapted from radio localisation. The present study expands on this work, and uses Cross Correlation (CC) to generate Time Difference of Arrival (TDOA) matrices for the responses of multiple sensors in a single multi-sensor array. The time delay estimates are provided here by calculating the cross-correlation between the whisker signals and searching for the time-lag that maximizes it. Multilateration of the time delays then provides the DoA.

3.3 Methods

3.3.1 Vortex ring generator

The vortices tracked in this study were generated using a simple vortex canon (side length 200mm), modelled on the vortex canon used in the Rostock study on live sea lions (Krüger et al. 2018), designed to mimic disturbances typical of swimming prey (Drucker & Lauder 2002). A spring loaded plunger as shown in fig 3.1 strikes the elastic membrane on the back, which then transfers the momentum into the formation of a vortex ring at the circular opening at the opposite site. The vortex generator is installed in a water channel with free surface, used here as a simple water tank with no flow. Each push with the plunger on the membrane creates a vortex ring (outer diameter Do = 40mm, toroidal core diameter Dc = 24mm see fig 3.2), travelling towards the model head at a speed of roughly $U_0 = 1.1 \pm 0.1$ m/s,

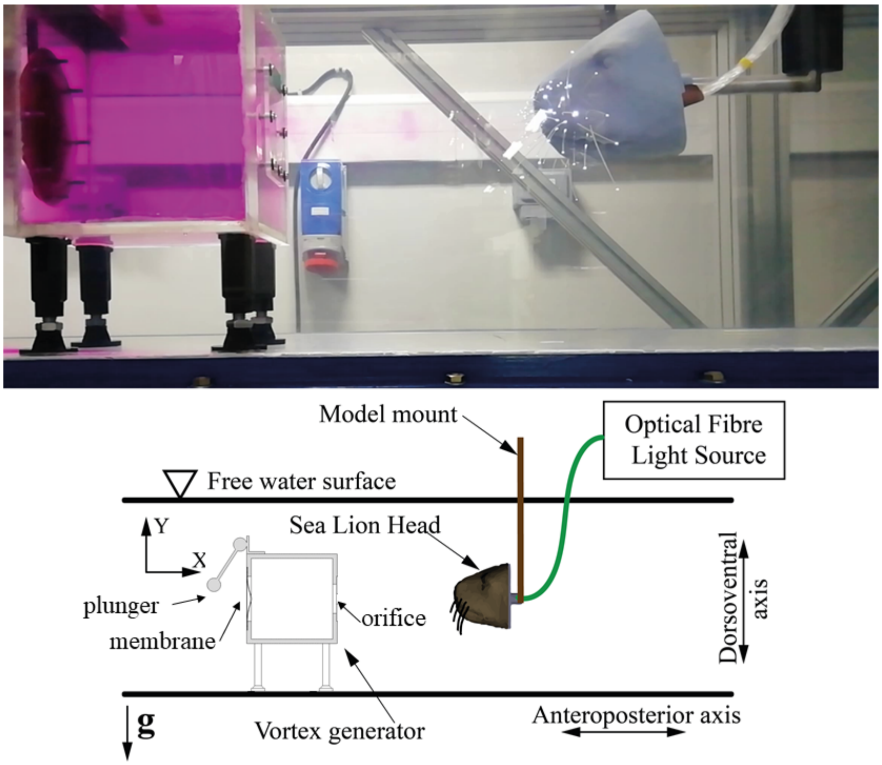

Figure 3.1: Top: Picture of the experimental setup showing the vortex ring generator filled with pink dye, 200mm away from the model of the sea lion head with its 3D array of whiskers. Bottom: principle sketch of the experiment, including the definition of the body axes .

calculated using high speed footage of a dyed vortex ring fired along a ruler. The speed drops slightly across the length of the model due to the interaction with the displacement body. Because of the short distance between the array tips (¡0.05m) it is considered to be constant along this scale. A visual impression of the vortex ring is obtained from food dye, which is added to the water within the cavity of the vortex canon and is entrained into the vortex ring during generation. In addition, for further visualization of the flow pattern around the travelling vortex, small tracer particles (Potters Industries, conduct-O-Fil silver-coated ceramics, diameter 80micron, PA, USA) were added to the water along the expected path of the ring. A typical picture of the disturbance flow pattern in the otherwise quiescent environment is given in fig 3.2 by means of a multi-exposed image of those tracer particles when illuminated with a light-sheet (Hardsoft, PL, IL-105/6X Illuminator). The flow field can be processed by the method of Particle-Image-Velocimetry, for further details see our previous paper (Muthuramalingam & Brücker 2019).

For the 3D array studies, the vortex generator is rotated around the model in the horizontal plane to simulate vortices arriving from various angles, testing the contralateral interaction with the sea lion model as depicted in fig 3.3. For the

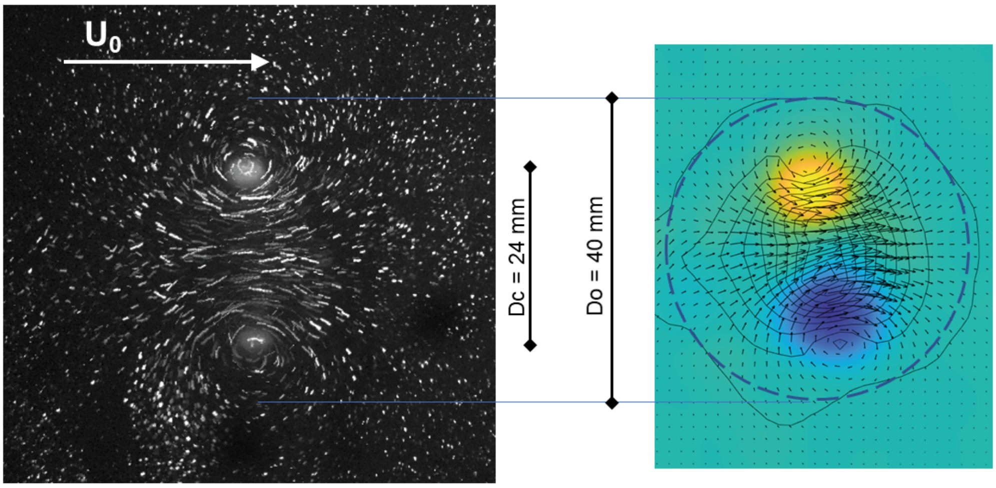

Figure 3.2: Left: Multiple exposure visualisation of the vortex ring in the horizontal plane. Right: In-plane velocity vector field induced by the travelling vortex ring. The additional contour lines show the velocity magnitude and start from 1/10 U_0 in steps of 1/5 U_0, where U_0 is the travel speed of the vortex ring. The color-coded vorticity field highlights the cores as regions of highest magnitude of vorticity, which represent the cuts through the toroidal core of diameter $D_c = 24$mm. The dashed circular ring approximates the outer diameter D_o of the ring, beyond which fluid has remained nearly stagnant with velocities lower than 1/10 U_0.

2D array experiments the vortex ring generator is kept stationary, but instead the model, placed in the same position as the seal head, is rotated around its vertical axis to simulate the different angles of arrival to the vortex generator.

3.3.2 Sea lion model with 3D whisker array

This experimental model is the same as described in our previous work (Elshalakani et al. 2020, Muthuramalingam & Brücker 2019) and the key features are described herein again. We use a 1:1 scaled model of the head of a sea lion with artificial whiskers (optical fibres with circular cross-section of diameter $d = 0.75$mm). The fibres are placed along the head with their origin at similar positions to the biological example and point outwards with a similar length variation. In addition, the material of the fibres has an elastic modulus, and diameter, similar to the natural whiskers. The array of optical fibres are inserted through holes from the backside of the 3D printed model and are illuminated from one end by an LED source such that the tips of the free fibre ends appear as bright spots, on both sides of the head. The fibres therefore represent one-sided clamped flexible cantilever beams with circular cross-section, interacting with the flow.

3.3.3 Planar surface with 2D regular whisker array

Another experiment is done with the same type of optical fibres arranged now in a regular array to provide reference data for a more simplified situation (compared to the artificial sea lion head). Therefore, a flat disc is used in horizontal alignment, which has clamped 13 optical fibres of a length of 100mm, pointing downwards along their vertical axes.The artificial whiskers are all arranged parallel to each other within a regular Cartesian grid pattern with a side length of 40 mm between two fibres and with the tips all lying in the same plane. The water tunnel and vortex generator are arranged as shown in fig 3.4, and fig 3.7. The interspacing between the fibres is chosen such that the circular-shaped disturbance pattern induced by the vortex ring (see fig 3.2) is always overlapping an area of minimum 3 whiskers simultaneous at each location within the grid. The disc with the fibres can be freely rotated on its mount around the vertical axis.

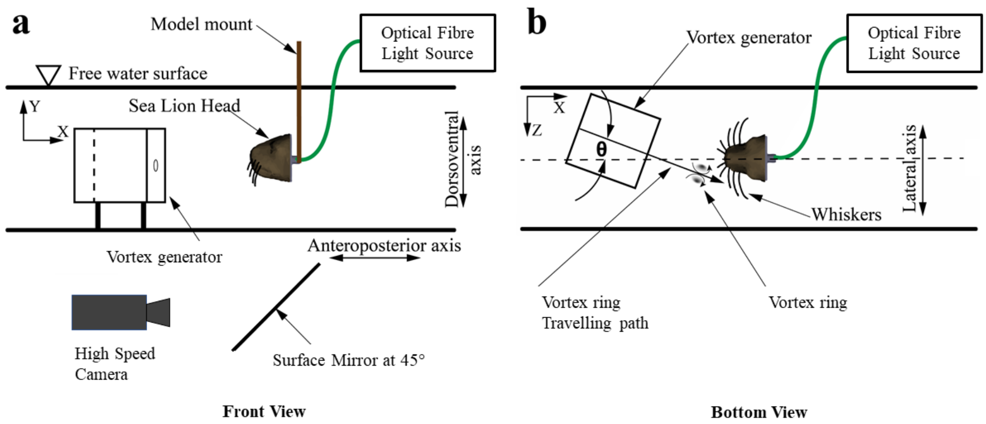

Figure 3.3: Schematic diagram of the seal head experimental set-up. To test different contralateral angles of impact, the vortex cannon is rotated around the head in between measurements. $\theta = 0 - 45\,\mathrm{deg}$.

3.3.4 Experimental setup for motion tracking

The tips of the optical fibres were tracked using a high-speed camera (ProcImage 500-Eagle high-speed camera) at a sampling rate of 250 Hz, as shown in fig 3.3. It has a pixel resolution of 1280 x 1024 which relates to physical dimensions of 221 x 177 mm. The built-in function in the camera calculates the Cartesian tip coordinates of each

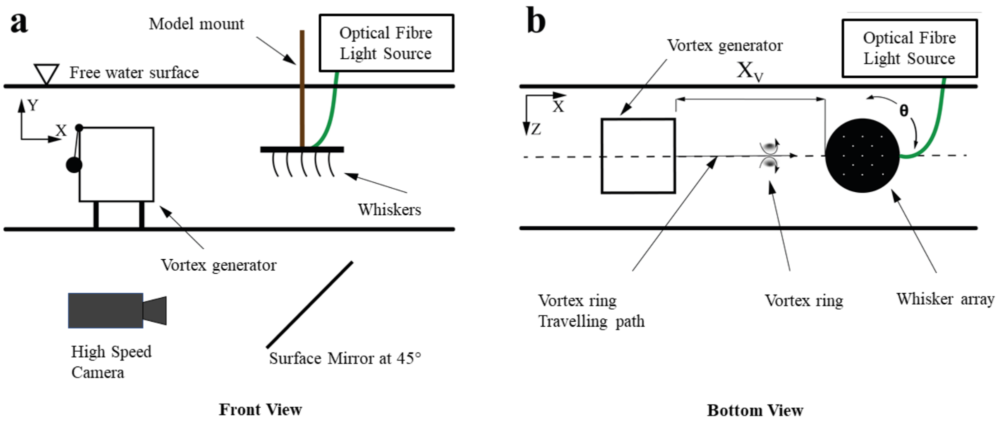

Figure 3.4: Schematic diagram of the 2D whisker array experimental set-up. To test different angles of impact within the array, the round disc housing the whisker array is rotated around its vertical axis. $\theta = \pm 45\,\text{deg}$.

light spot automatically using the barycentre mode. The measured signals are the magnitude of tip deflections (Euclidian norm) of each of the optical fibres captured simultaneously, which is directly proportional to the applied bending moment at the shaft of the whiskers (Euler–Bernoulli beam theory) (Elshalakani et al. 2020, Muthuramalingam & Brücker 2019). This system was used to track the sensors on both of the models. Note that the camera viewing position ensures the capture of the major components of the tip displacements, but for the 3D array the optical tracking of the tips only can capture the projection of the displacement vector, which is in the direction of the travelling vortex. A full description of the displacement vector in all directions would require an additional camera looking from another viewing direction in a stereo-camera arrangement, for which an additional camera was not available.

The maximum variation in the tracking software's reported position of an undisturbed sensor tip due to background noise is 0.5 px, which is very low. This stems from uncertainties in the tracking code and scattered light. When this noise is compared to the smallest tip deflections on signal arrival, measured at roughly 15 px, this still gives a high Signal to Noise Ratio (SNR) of at least 30.

3.3.5 TDOA from Generalised Cross Correlation (GCC)

Using the generalized cross-correlation (GCC) algorithm, or derivatives thereof, is a widely used method for the TDOA estimation (Nagy 2016, Dubrovinskaya & Casari 2019). Here we consider a pair of whiskers being disturbed by a hydrodynamic signal.

The signals used in the GCC of each pair of whiskers are defined as:

$$W_1(t) = s(t) + n_1(t) \tag{3.1}$$

$$W_2(t) = s(t + D) + n_2(t)$$

where W denotes a whisker, s is the recorded signal given off by the source, D is the time delay, and n is random, uncorrelated, measurement noise. The sources of measurement noise present are scattered light from the fibre tips and the uncertainty in the tracking camera's centring predictions. Therefore, for each whisker the signal is the recorded position of the whisker tips.

The true value of the GCC is obtained via(Knapp 1976):

$$R^{(g)}_{w1w2}(\tau) = \int_{-\infty}^{\infty} \psi_g(f) G_{x_1x_2}(f) e^{j2\pi f\tau} df \tag{3.2}$$

where $\psi_g(f)$ is the general frequency weighting, and $G_{x_1x_2}(f)$ is an infinite observation of the signal.

Hence the GCC between W_1 and W_2 for a finite signal 't', is estimated as:

$$\hat{R}^{(g)}_{w1w2}(\tau) = \int_{1}^{t_{max}} \psi_g(f) \hat{G}_{x_1x_2}(f) e^{j2\pi f\tau} df \tag{3.3}$$

where $\hat{R}$ represents an estimate of the GCC when R is evaluated for the finite series of $x_{1,2}(t)$.

The maximum value of $\hat{R}$ corresponds to the delay, D, or TDOA, between each whisker pair. These calculations are repeated for each whisker pair, and therefore this GCC function outputs the set of time delays between every pair of whiskers in the array.

3.3.6 DoA Calculations in 2D

The Direction of Arrival is the defined as the angle between the oncoming vortex ring and the anteroposterior axis of the model, in the horizontal plane. The bow-wake effect of the travelling vortex ring is causing the initial deflection of the whiskers and is approximated across small distances as a signal propagating with a planar wavefront. This approximation is well supported by PIV measurements of the vortex ring. Figure 3.2 shows that the fastest moving parts of the flow form a rough line across the front of the ring.

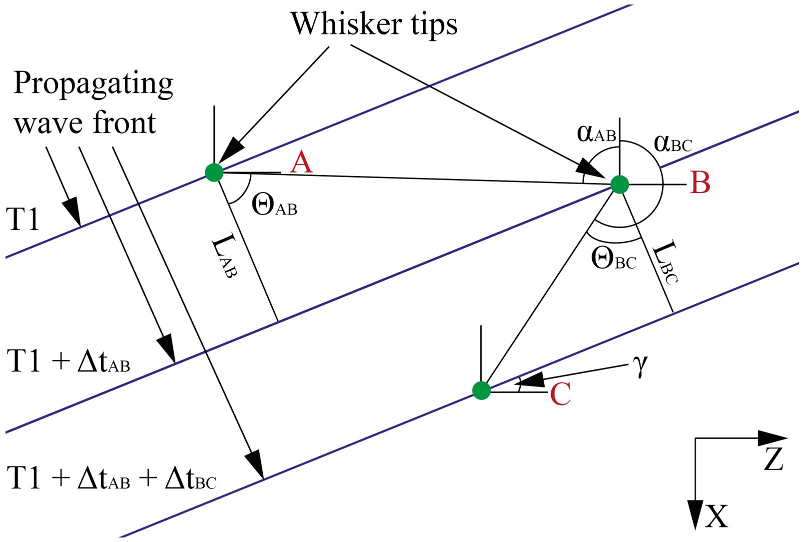

Figure 3.5: An example triplet of whisker tip points, showing how TDOA multilateration calculations are adapted for this purpose. The blue lines represent the position of the bow wave front, as it passes by and disturbs the sensors.

The inputs to the multilateration function are the arrays of time delays between every pair of whiskers, and the X and Y position of each whisker tip while the whisker is at rest. The time delays are calculated via the aforementioned GCC, as a function of the whiskers displacement (see above).

The calculation relies on the basic principle of TDOA multilateration. The following data processing is similar to passive sonar or other audio localisation microphones (Ollivier et al. 2019). It differs from these conventional usage cases in that both the time of the signals emission, and the speed of the signal are unknown. To account for this, herein triplets of sensors are used instead of the conventional pairs (Luke & McAlpine 2019), used when the speed of the signal, or the signal emission time are given. This allows for the calculation of the DoA by comparing the ratio of the TDOA with the ratio of the distance between the sensors, a comparison that is independent of the signal's velocity or time of emission.

Assuming that the direction and velocity of the signal remain constant when traveling over the triplets, looking at the time difference between the excitation of three whiskers of known positions should produce the angle and velocity of the signal as follows (notation follows fig 3.5):

$$\frac{\Delta T_{AB}}{\Delta T_{BC}} = \frac{L_{AB}(\gamma)}{L_{BC}(\gamma)} \tag{3.4}$$

where 'ΔT' is the time difference between the whiskers A and B, and 'L' is the distance between points A and B in the direction of travel.

$$L_{AB}(\gamma) = cos(\Theta_{AB})\sqrt{(x_B - x_A)^2 + (z_B - z_A)^2} \tag{3.5}$$

The coordinates 'x' and 'z' represent the pixel positions of whisker tips A and B, and Θ_{AB} is the angle between L_{AB} and the line AB:

$$\Theta_{AB} = 180 - \gamma - \alpha_{AB} \tag{3.6}$$

where 'α_{AB}' is the angle between the distance vector $\vec{AB}$ and the z-axis, and 'γ' is the angle of the propagating signal front.

To find the solution, an algorithm is applied that scans all possible values of γ, from -90 to 90 degrees in 0.002 degree increments, recording the range of values of γ that satisfy equation 3.4 to four significant figures. The size of the range of resulting values provides an estimate of the uncertainty in the angle output of that whisker triplet, and is mostly dominated by the size of γ, as small angles result in small time delays between whiskers in the triplet, which are therefore more sensitive to random error. This is repeated for all possible triplets of whiskers, and the result is taken from the displacement-weighted average of the γ outputs:

$$\bar{\gamma} = \frac{\sum_{n=1}^{m}(\gamma_m * \frac{MinD}{\bar{D}})}{m} \tag{3.7}$$

where 'MinD' is the minimum displacement of any whisker in the triplet, and '$\bar{D}$' is the average whisker displacement across all measurements.
The travel velocity of the signal is therefore simply estimated as:

$$\hat{V}_s = \frac{\sum_{n=2}^{p} \frac{L_{1,n}(\bar{\gamma})}{\Delta T_{1,n}}}{p-1} \tag{3.8}$$

where $L_{1,n}(\bar{\gamma})$ is the length between points 1 and n, at the calculated $\bar{\gamma}$, and $\Delta T_{1,n}$ is the corresponding time delay. Error in the travel velocity due to recorded vertical variation in vortex exit angles ($\pm 2.7°$) is calculated as follows:

$$\%Error = \frac{\hat{V}_s - \hat{V}_s * Cos(2.7°)}{\hat{V}_s * Cos(2.7°)} * 100 \tag{3.9}$$

Lowest recorded velocities were roughly 1 m/s, leading to a maximum error of 0.11%.

3.4 Results

Figure 3.6 shows the interaction of the vortex ring with a tandem pair of whiskers in the 3D array, which are both roughly arranged in the horizontal plane and in line with the horizontal travel direction of the vortex. For simplicity when dealing with the sea lion model, only the interaction along the head in the horizontal plane crossing the mid section of the head is tested, while the angle of impact is varied in this 2D plane. Only the whiskers which are near to each other, along the path of the vortex, and have similar length, are used for the source localisation. The time-series of the spots of the whisker tips clearly highlights the response to the bow wake of the incoming vortex ring. The leading whiskers reacts first at 1s after the pulse initiation and the trailing one reacts 0.12s later with a longitudinal shift of the same order as the leading one. This time-difference demonstrates the feasibility of using the tip displacement signal to determine the TDOA in the pair of whiskers. The two whiskers spotted in the figure are part of a triplet which is used to calculate the DoA with the above method. Compared to our previous studies described in (Muthuramalingam & Brücker 2019), there is no clear jerk-type motion of whiskers during the passing of a vortex. Here, the momentum of the fired vortex rings dominates the whiskers' motion by flow-induced drag in an otherwise stationary flow field. This is different to the situation when vortices are convected in an established flow past the whisker as in the wake of a cylinder used in (Muthuramalingam & Brücker 2019), where the whiskers show a stronger response to the pressure field. Additionally, the vortex ring's induced pressure field has a toroidal shaped core of low pressure, while the von-Karman vortices generated from a cylinder have a rather tubular axial core of low pressure. This aspect influences the interaction of the filamentous whiskers with the pressure field.

Another visualisation of the interaction is given in fig 3.7, which shows a close-up view of the vortex ring interacting with a triplet of whiskers making up part of the regular array. The vortex ring is visualised by combining tracer particles and photo luminescent dye to show its shape and wake. In addition, typical whisker tip displacement profiles (relative to zero flow) are shown, to illustrate the response to the flow event passing by. The displacement magnitude includes the motion of the tips in two dimensions (longitudinal and transversal) as they interact with the vortex ring. The leading whisker W#1 is first laterally deflected by the rotation

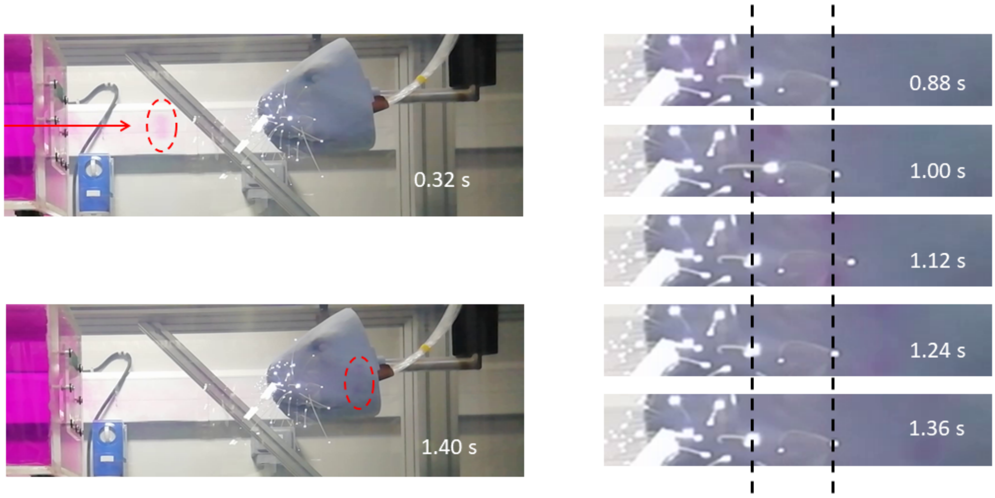

Figure 3.6: Picture of the 3D printed sea lion head with integrated optical whiskers, seen by the bright spots at the tips. The time series on the right-hand side with zoom-in illustrates the successive excitation of two neighbouring whiskers in the same horizontal plane when hit by the travelling vortex ring (travel direction from left to right).

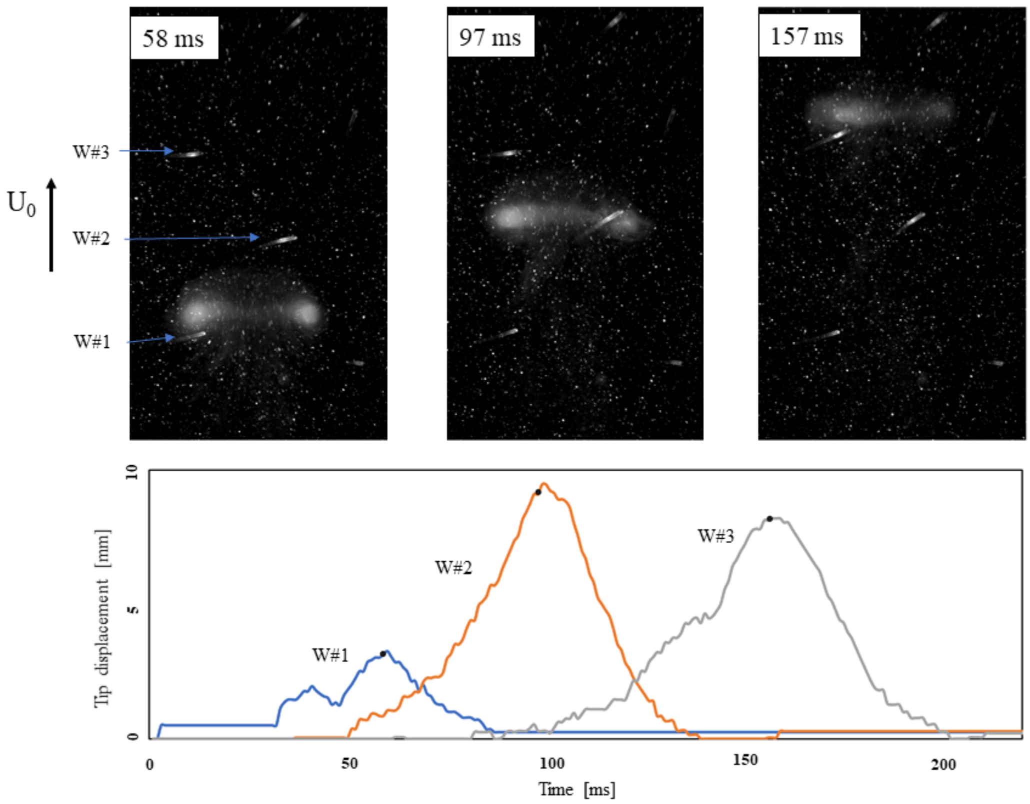

Figure 3.7: Top: Vortex ring propagating across the array. Bottom: Whisker tip tracking data matches the visualisation of the vortex ring.

of the vortex ring before drafting into the wake and moving forward with it. This interaction results in two successive peaks in the profile of W#1, the first reflecting the rotation and the second the drafting. Successive peaks in the profiles correspond to successive deflections of whiskers W#2 and W#3. All these motions are accounted for in the CC, which solves for the best fitting TDOA.

The processing of this data results in calculated values of the DoA angle versus the imposed vortex ring travelling direction, shown in fig 3.8. Displayed on the top are the results for the whisker array mounted on a flat plate (fig 3.8A) compared to the results for the seal lion model on the bottom (fig 3.8B). The error bars depict the uncertainty in the calculated DoA, which is dominated by poorly resolved triplets due to small angles of incidence (γ), or triplets affected by random motion in the vortex ring's wake. On the flat plate model, all the whiskers are evenly spaced, the same length, and positioned perpendicular to the incoming vortex rings (see fig 3.4). Consequently, the position along the whisker at which the vortex impacts is roughly the same for all whiskers involved. The vortices fired with a maximum recorded vertical variation of $\pm 2.7°$to the horizontal, which even at the vortices slowest speeds, lead to a very small error of 0.11% in the calculated speed of the vortex ring. The directionality calculations based on the whisker triplets show a reasonably good trend with the imposed impact angle (linear regression with R^2=0.96). This idealised setting demonstrates the effectiveness of multilateration principle applied to the whiskers when detecting the DoA of a vortex ring, evidenced by the results outside of small incidence angles.

For the seal lion model, the results shown in fig 3.8B show higher uncertainty in the calculated DoA, and the correlation of the trend (linear regression with R^2=0.78) is not as strong as for the regular array. There are several contributing aspects. Firstly, the model has the whiskers retracted, with their length increasing from the nose to the downstream part of the muscle pad, approximating the natural arrangement of the vibrissae (Muthuramalingam & Brücker 2019). This leads to uncertainties in the position along the length of the whisker that the vortex core is impacting. This can induce an error as the calculation is based on the relative position of the tips to each other within the array, and assumes that the tip is always the first part of the whisker to be pierced by the ring. We tried to reduce this uncertainty by carefully arranging the model such that the vortex brushes past the longer whiskers, and then only considering those longer whiskers in the calculations. This reduces the number of valid triplets and increases noise. Another source of uncertainty is the possible out-of-plane component of the tip motion, which the camera is not able to detect. Therefore, the measured signal may not represent the total amplitude of tip motion other than in the case of the planar array. This effect is considered to be of lower influence.

3.5 Discussion and Conclusions

We have shown via a physical demonstration, that an array of whiskers can be used as a reliable system of sensors for determining the DoA, via noise resistant GCC algorithms (Glick et al. 2021, Ollivier et al. 2019), multilateration of triplets of whiskers, and using data processing methods adapted from audio and other source localisation techniques. The relevance of this study is related to the previously reported sensing capabilities of sea lions exposed to a traveling vortex ring, passing one of the vibrissal pads on their heads (Krüger et al. 2018). Consistent results of DoA detection were obtained using a similar setup with a vortex ring generator, and simplifying the system to an array of whiskers of the same length and with regular spacing. When using cross-correlation time-delay estimation with a pulsed signal, the rising or falling edge of the signal can be used as a reference mark for the time of arrival for the CC. Taking the difference in the time of arrival gives rise to the TDOA. A triplet of three sensors with two TDOA measurements are the minimum number of measurements required to calculate the DoA in a 2D plane, without knowledge of the vortices' velocity or time of emission. This demonstration supports the idea that multilateration processing could be a method employed by the animal to detect the travel path and velocity of such disturbances.

Our results from the regular array were more consistent than from the seal head model. We explained the higher noise present in our seal head model by the fact that the whiskers in the model are retracted in the streamwise direction, which induces uncertainty in the position at which the vortex ring impacts the whiskers along their length. The calculation method assumes that the tip is the first part of the whisker which is piercing the vortex ring, which is only guaranteed to be the case with the whiskers protracted forwards. This is still open to be studied in a future experiment with a new model with protracted whiskers, supported by the observation that seal lions protract their whiskers when actively tracking (Milne et al. 2020). It is worth considering, that studies into the minimum hydrodynamically perceivable angle of seals (Krüger et al. 2018) demonstrate that the reliability of the seals' interpretation of the DoA drops for angles below 20 degrees. This aligns with measurements for

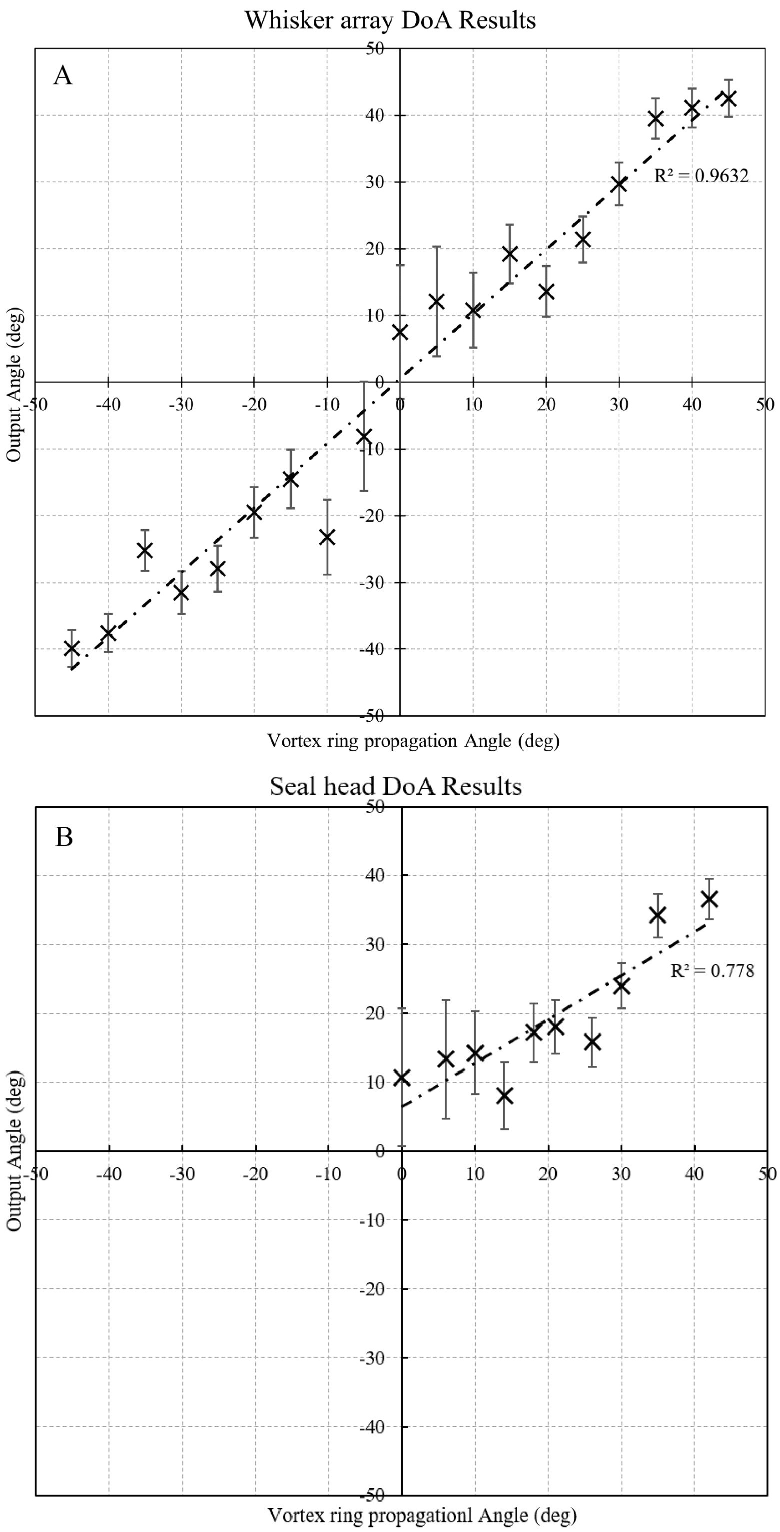

Figure 3.8: Calculated DoA angle using multilateration versus the vortex travel direction. Error bars indicate the range of DoA predictions produced from 50+ different whisker pairings per angle, from a single pulse. A: regular array on the flat plat for a full 90 degree arc (Top). B: array on the sea lion model tested for single-sided contralateral pad impact at angles from 0 - 45 degrees.

the bio inspired whisker arrays in this study, with larger uncertainties at these small angles.

This aside, a regular array attached to a plate is a more practical deployment of the sensors for future applications, including autonomous underwater navigation and tracking systems. Taking multiple triplets of sensors leads to an over-determined system, which produces more accurate solutions by combining the output of all suitable triplets. In addition, machine learning or training methods may further improve the systems reliability, and reduce its sensitivity to noise. The regular pattern of the array was used as a simple layout to ensure the vortex pulse could be picked up reliably. Here, the size of the vortex ring was known, and the array was chosen such that it had sufficient spatial resolution to detect the signal with a number of triplets.

In future studies, when such an array is deployed to measure signals of unknown size or duration, and where therefore every additional valid triplet of whiskers would improve the results, one could use more specialised array layouts adapted from acoustic directionality studies (Mortsiefer & Peissig 2017). These spiral array layouts use careful spacing of a multi-armed spiral to help maximise the number of useful whisker triplets that can be used reliably by avoiding very small angles of incidence with the oncoming signal or between whiskers in the triplet. For applications where the use of multiple sensors, arrays, or decentralised arrays would be beneficial, the directionality calculation functions could be expanded to utilise some form of Kalman filter to better combine readings from multiple sensors, reducing the least squared error (Okello et al. 2011).

Applications of these techniques are manifold. Important is that such sensing would be beneficial in the near-field range to detect objects passing by, or to sense topographical structures due the wall-effect when moving along close to the ground. In such applications considerations must be made for the impact of multi-phase flows, with particles and debris typical of flows close to the ground. Moving forward we look to investigate the performance of our system in such an environment.

3.6 Critical Analysis

In the study above we used lines of best fit, and the R^2 values thereof, to assess the performance of the arrays, and the quality of their measurement. While this can be useful to assess the system's tendency to skew the readings one way or the other, it is not a particularly good metric for assessing the quality of the system's predictions, nor the best way to compare the relative performance of different arrays, or of one arrays performance under modified conditions. Instead, as used in our subsequent publications, RMSE is a more representative measure of the system's overall performance. Calculating the RMSE of the predictions for both models nets 6.34° RMSE for the seal head model, and 5.28° for the flat plate. This clearly shows the higher accuracy of the flat plate array, and provides a good frame of reference for the significant performance improvements achieved by further refinement of the arrays and approaches in subsequent studies.

In the study above, vortex rings are treated as a planar wave front. This is a large oversimplification that was partly accounted for by identifying and removing the whiskers at the edge of the vortex that produced the most error as a result of this oversimplification. This had had the additional benefit of accounting for another phenomenon which disrupted the analysis. whiskers at the edge of a vortex would undergo a 'double displacement' whereby the initial displacement as a result of the bow wake was weaker, and the counter flow on the outside of the vortex ring would displace the whisker tip back past its starting position into a second, similarly sized displacement peak, before the whisker would revert to the normal post disturbance damped oscillation. This pattern made CC with a central whisker that displayed only a single major peak difficult, as the correlation with the second peak was often stronger and would therefore produce incorrect, very late, time estimates.

This can all be accounted for on a second pass, after the first pass provides estimates of the speed and path of the disturbance. The size of the disturbance can be estimated by looking at how many, and which, sensors are disturbed. If the entire array is disturbed then a planar wavefront can be assumed as above with minimal error. Where the array is partially disturbed, the radius of the disturbance can be estimated by looking for the largest distance normal to the path of the vortex, between two disturbed sensors. With good estimations for the radius, travel velocity, and path of the vortex, the TDOA matrix can be adjusted to account for the curvature at the front of the disturbance. Time offsets can be introduced for each whisker as a function of the distance to the centre of the vortex. The difference in distance from where the front of the disturbance was, versus where it was expected to be on the first pass, is known, and dividing this by the speed of travel gives the offset time for each whisker. This updated TDOA matrix can then be used to produce a more accurate estimate of the vortex path by using the whiskers that were previously filtered out, and corrects for the planar wavefront assumption.

General questions raised by reviewers

1. **How similar are the fibres used in the sea lion model to the real whiskers?**

   There are many important features of real whiskers that have been removed or simplified for this experiment. The length of the whiskers was closely modelled on those of a real seal lion. The complex twisting undulating elliptical shape of real whiskers can in no way be represented by the circular cross section of the fibres. One of the key variations is in the thickness of the whiskers. The thickness of real whiskers tapers towards the tip, and thus longer whiskers are generally thicker at the base than shorter whiskers. This tapering results in increased flexibility towards the tip but this is partly counteracted by a corresponding increase in the elastic modulus towards the whisker tip (Quist et al. 2011) as seen in some animals. The mean diameter and elastic modulus of the fibres is close to those values reported in literature for live sea lions. Therefore, the longer fibres have a very similar mechanical response to that of the longer whiskers, but the shorter fibres are very rigid compared to the shorter whiskers.

   On top of this, unlike in an animal, where the whiskers are supported by muscles that feel the forces in the whiskers, the whiskers in this study are clamped at the base. Therefore while a sea lion might still feel forces on a whisker that doesn't bend, our setup cannot detect this. The result of this is the highly reduced utility of the shorter whiskers. The arrangement of whiskers in nature, particularly pinnipeds, often follows grid like patterns (Woolsey et al. 1975). This was not closely mimicked by the model seal head, in part due to the non uniform curvature of the whiskers.

The highly reduced utility of the shorter whiskers, and the nature inspired whisker grid layout were the primary factors in the selection of longer whiskers in regularly arranged plate array.

2. **How would deviation in the mechanical properties affect the result of the study?**

   As stated above, the longer artificial whiskers have a very similar mechanical response to the real whiskers, aside from the simplified shape. Studies into the benefit of this unique shape (Hanke et al. 2010, Valdivia y Alvarado et al. 2012) largely agree that the main benefit of this geometry is increased sensitivity via reduction in VIV and/or increased sensitivity to key frequencies. It follows that all results from this study could benefit from increased sensitivity and would be improved by making use of this geometry, but the key underlying principles and methods would remain exactly the same.

   Producing highly accurate copies of seal whiskers with the required fibre cores and the desired mechanical properties is currently unfeasible and we do not believe that this would significantly alter the hypothesis or results of this study.

3. **Are all the fibres the same length/diameter? It makes sense that the real whiskers are not all the same length/diameter, which makes them respond to slightly different frequencies.**

   All model fibres are the same diameter, although some are longer than others, modelled on a scan of a real seal head. The way we look at the whiskers' responses in this study is almost like a step-response and we are therefore not studying it as a frequency-based excitation. The hypothesis and results of the present study is therefore not sensitive to the precise frequency ranges that real whiskers are most sensitive to. There is perhaps some additional sensitivity that could be gained by using a range of whisker lengths, but this is unnecessary where we are in control the emitted stimuli.

4. **How is the noise level of "0.5px" calculated from an image/images.**

   The position of the whisker is taken as the geometric centre of the recorded light spot, which enables the sub-pixel measurement of the whiskers position. The stated noise level is therefore calculated as the maximum range of positions reported for a stationary whisker tip (e.g. the tracking code reported X values ranging from 127.4 px to 127.9 px, while the whisker was undisturbed).

5. **When considering fig 3.7, to what extent does the deflection magnitude of the whisker influence the accuracy of the time delay produced by CC. Larger displacements seem to result in a later peak displacement, presumably after the point at which the stimuli has passed the starting (undisturbed) position of the whisker, which is taken as the location of the time delay for the multilateration. Does this later peak displacement have a noticeable influence on the TDOA matrix and/or the angle estimation?**

   The true time of arrival of a stimulus is somewhere on the rising edge of the deflection peak. When the energy of the stimulus is greater (or a whisker is hit directly rather than glancingly), the whisker deflects ahead of the stimulus due to its bow wake, causing some uncertainty in the true arrival time of the core. The whisker is also dragged along for longer, resulting in a later peak deflection, and longer time taken to return to the rest position. The point of maximum deflection is therefore a more accurate estimate of the time of arrival for weaker deflections than it is for larger deflections. Cross correlating deflections of similar magnitudes causes little error in the time delay estimates as this delay is mimicked by both whiskers. Cross correlating deflections of dissimilar magnitudes causes an over or underestimate of the travel time between the whiskers. Significant underestimates of travel time produce unreasonably high travel speeds, and are usually very easy to spot and filter out automatically. Over estimations are more of a problem as they are harder to identify as errors. This causes some errors in the TDOA matrix, and likely contributes to the error in the direction prediction. This is not however a major concern as the number of whisker combinations used in the multilateration enables this to be mostly averaged out.

Studies relevant to the paper

Kundu (Kundu 2014) discussed a number of techniques for solving sensor array based acoustic source localisation problems under various conditions, one of which presents an approach that is reminiscent of the concept used herein. The author goes on to describe an error function optimisation method to determine the source location, in absolute terms, based off the TDOAs, which could be adapted for other hydrodynamic sensing purposes. The author raises the point of the inherent uncertainty present in all experimental methods. Kundu acknowledges the success of Niri et al. (Niri & Salamone 2012) who used an extended Kalman filter to remove this noise and produce iterative estimates of the source location in a probabilistic model, but doesn't discuss how or to what extent this would benefit the methods presented therein. The titular study above struggled to benefit from the addition of a Kalman filter, but the lack of detailed reporting on its application or any benefits thereof, suggests that this method should not expect a significant improvement with its inclusion.

Liu et al. (Liu et al. 2024) proposed a style of pressure sensor seeking to emulate the lateral line system seen in fish. They used their aerofoil shaped pressure sensors to construct a small, 6 element, sensor array. Despite the different sensor design, they sought to make use of similar methods of signal CC to determine the path of an object moving past the array. Their array was sparse, rather than concentrated, and as such could only detect the presence of the passing object one sensor at a time. Therefore, comparing the signals of each sensor was more about reconstructing the path taken across the array, rather than providing a reading of an object's instantaneous location and heading. Nonetheless, this is one of a growing number of studies looking at array based sensing of hydrodynamic effects, showing increased interest in the field.

Dunt et al. (Dunt et al. 2024) conducted a numerical study on the effect of undulation wavelength to whisker diameter ratio (λ_u/D_w) on reducing unsteady lift forces in the vicinity of a whisker, and found an order of magnitude reduction at λ_u/D_w ratio of 3-7, with a minimum unsteady C_L value at around 3. they also observed a significant drop in Strouhal number within this region.

Kamat et al. (Kamat et al. 2024) conducted numerical and experimental analyses of the proficiency of pinniped whiskers in reducing VIV. They found that undulations and the other geometric features suppressed VIVs most effectively at a λ_u/D_w of 4.5. Experimental study of the whisker found that such a whisker produced 13 times less VIV noise than a cylinder. This represents a significant drop and emphasises the remarkable properties of the seal. These studies, among others, emphasise the value of finding a way to integrate these geometric features into future artificial whisker sensor projects.

Chapter 4

Tracking hydrodynamic disturbances with fibre-optic whiskers

4.1 Abstract

Previous research has identified the capabilities of artificial whisker sensor arrays as an innovative method of tracking and evaluating flow events and disturbances. In this work, a new approach is put forward, focusing on achieving enhanced sensitivity and improved performance of fibre-optic whisker sensors, based on the principle of fibre Bragg Grating (FBG) based optical stress sensing. Its performance is evaluated against more simplistic approaches, and previously demonstrated methods of optically tracking the tips of whisker sensors. The study has found the performance and sensitivity of these FBG-based sensors to be very satisfactory, with sufficient sensitivity to bending stresses to enable using Cross-Correlation (CC) and multilateration techniques (as evaluated in prior studies) to produce reliable Direction of Arrival (DoA) and velocity estimations, at a typical SNR of around 2 dB. The system has shown the capability for correction of potentially disruptive variations in temperature, allowing for effective measurement of the key hydrodynamic disturbances under study, irrespective of the local environmental conditions.

4.2 Introduction

With the increase in the use of unmanned or autonomous underwater vehicles, there is an emerging challenge in monitoring their environment more effectively. A challenge that demands an innovative approach to flow measurement technologies that are well suited to the challenges of the environment. In particular, when a large fleet of vehicles of this type is planned, additional demands are placed on the monitoring system, in terms of dealing with the surrounding hydrodynamic noise, both to avoid interference, and from the desire to detect quiet operators in the area. The disturbances of interest often take the form of coherent vortical structures, which both travel with the flow and are left in the wake of travelling objects such as marine life or ships. In earlier attempts to better observe different hydrodynamic disturbances, several groups have investigated the performance of simple artificial whisker sensors, either as single sensors (Zhang et al. 2021, Liu et al. 2022) or as an array of sensors that react to the flow environment (Xu et al. 2021, Glick et al. 2022), often drawing useful inspiration from nature (Adachi et al. 2022). For example some approaches mimic the way that seals track objects, despite not always having precise directionality and instead resorting to "undulatory" patterns in and out of their prey's wake (Schulte-Pelkum et al. 2007). The previous generation of whisker sensors has regularly suffered from problems with versatility, reliability, and ultimately their sensitivity. In particular, issues of versatility and reliability have been an issue for systems that rely on visual tracking methods due to interference effects from light pollution, the presence of visual obstructions, and difficulty mounting cameras in optimal locations, all of which need to be overcome without disrupting the flow itself. The reliability concerns that are familiar with the use of electronic sensors are typically their vulnerability to any moisture ingress (via leaks or high humidity), electro-magnetic disturbances, or saltwater corrosion, which is a particular problem with electronic sensors. Fibre optic sensors (which are non-electrical and passive in operation) are well suited to overcoming these issues, taking advantage of their inert nature and resistance to water exposure, saltwater corrosion, and electro-magnetic interference.

This study has aimed to enhance the tracking of hydrodynamic disturbances, a process that can be achieved through the design and evaluation of a new class of whisker sensors, designed by combining the well-known monitoring capabilities of fibre optic sensors, with our previously demonstrated adaptations of established source localisation techniques (Glick et al. 2021, 2022). The potential for using fibre optic sensors designed around FBGs, to be used as contact sensors has been explored in previous studies that used the deflection of a flexible sensor mount, to stretch the fibre and thus cause a wavelength shift (Heo et al. 2006). Further studies have used whisker-like FBG sensors for surface mapping (Zhao et al. 2017), imitating mammalian whisker use, and mimicking 'whisking' behaviour, for example as seen in rats (Jadhav & Feldman 2010, Morita et al. 2011). The approach used therein utilises the strain sensitive nature of FBG sensors and indeed has met with some success. The displacement of the whisker tip bends the fibre sensor, and induces a predictable and measurable wavelength shift for a given displacement. Thus by carefully monitoring and then calibrating this wavelength shift, such systems have successfully been used to assessed shaped obstructions and variations in surfaces in remotely controlled environments.

Recent review studies (Wang et al. 2023, Hollenbeck et al. 2023), have highlighted a multitude of methods relying on electronic and visual tracking, including mechanisms that offer solutions to the issue of camera placement (Kent et al. 2021), as well as advances in optical sensors used for self orientation (Wang, Yang, Wang, Jiang, Bai, Meng, Li, Geng & Sun 2023). These sensors rely on the changing interference signals of a multi-beam system as the cavity lengths vary when subjected to external stimuli, allowing for pitch and roll measurement.

Building on these previous studies, in this work an optical whisker design for flow sensing and event detection has been developed, that utilises a simpler and more advantageous detection premise. Here, the strain sensitive nature of the FBG sensors can be used to detect the bending motion of the sensors. Therefore the disturbance is seen in each of the sensors' signals, as the disturbance moves across the array. The path of the hydrodynamic disturbance can therefore be tracked by observing the shift in the temporal signatures across the array of whiskers. This allows for the calculation of the velocity and direction of the disturbance by observing the Time Delay of Arrival (TDOA) in the bending-induced wavelength shifts. Such a method removes the need for detailed sensor deflection calibration, and thus avoids any issues relating to changes in fluid density or viscosity.

In this study the performance of this system is assessed, investigating the sensitivity of the sensors, including how this affects the accuracy of the subsequent flow behaviour calculations, and the relative computational cost of this approach. The study also addresses the performance impact of the sensor layout and spacing in order to optimise the hydrodynamic sensor array.

4.3 Materials and Methods

Water tunnel arrangement

Two water flow arrangements have been used in the study, and both have used the same closed-circuit water tunnel, with a test section of 40 cm width × 50 cm depth × 120 cm length, as is illustrated in fig.4.1. Here it can be seen that the test section is transparent on all sides, allowing for visual observation of the flow behaviour, during the flow studies that are described in this paper. The model platform with the optical whisker array mounted on it was submerged in the water tunnel, along the centre-line of the test section in the mid cross-section as can be seen from the figure. A series of test arrangements was set up and in the first of these, tests were conducted in water which was initially stationary and then disturbed by vortex rings. The ring vortices had an outer diameter of 40 mm, core diameter of 28 mm, and an initial velocity of 100 cm/s. These types of disturbances could be created using a vortex cannon in a reproducible manner. A similar vortex cannon was used in previous studies to test the sensing capabilities of live seals (Krüger et al. 2018), where the size and speed of the vortex ring used mimics those vortices left in the wake of prey fish in nature (Hanke & Bleckmann 2004). The vortex ring generator orifice was positioned 200-300 mm away from the front of the sensor array. This allowed for a direct comparison with the performance of a previous fibre optic sensor design from the authors (which was tested with the same equipment under similar conditions (Glick et al. 2022)).

The second arrangement used involved tests conducted in flowing water where the flow disturbances were produced by a vertically oriented cylinder with a 30 mm diameter, placed upstream of the sensors. The cylinder was used to consistently shed turbulent vortical flow features, which pass the sensor array at about 2 Hz, (per the Strouhal number of 0.21). In keeping with prior studies, the cylinder used was positioned at a series of distances in front of the array, from 10Dc (1Dc = 1 Cylinder Diameter) to 25Dc (300 - 750 mm), and the mean flow speed was varied from 10 to 25 cm/s. This approach again built on previous work from the authors,

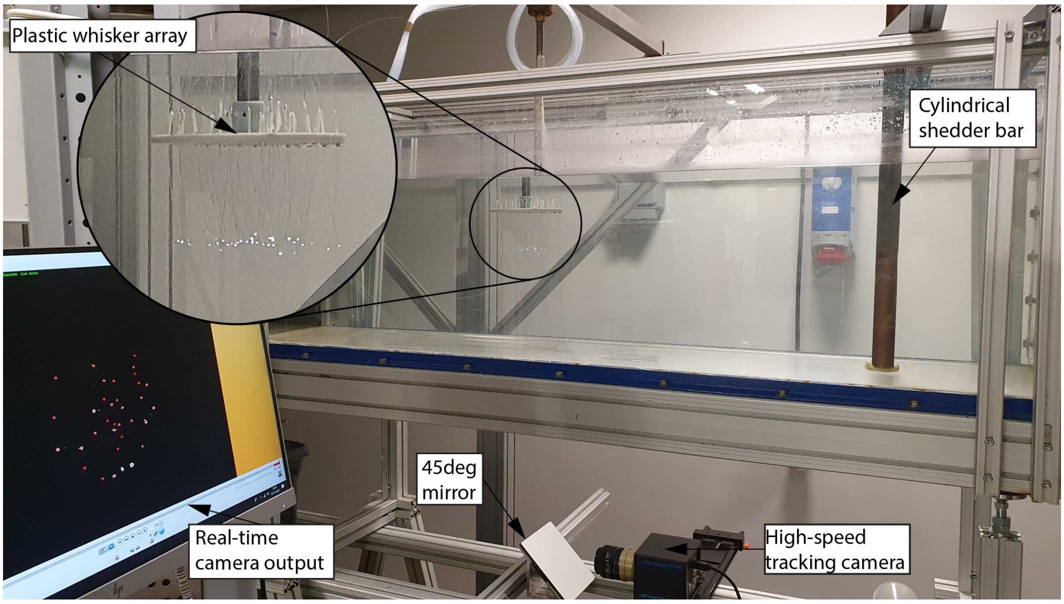

Figure 4.1: Pictured is the experimental setup for flow disturbances in established flow, using a spiral array of visually tracked plastic fibre whiskers

in that way allowing for a direct comparison of the performance (Glick et al. 2021).

When submerged into the flow, the bending of the slender fibres (mimicking the whisker) shows a mean bending component, which arises due to the drag of the stationary mean flow – this is a component which does not change over time. When a turbulent vortical flow feature in the flow was seen to pass the fibre, it induced an additional fluctuating part of the bending. It had been previously observed (Muthuramalingam & Brücker 2019, Glick et al. 2022) that there are two components contributing to the vortex-induced fluctuating motion. The first was the velocity-induced drag component, which is proportional to the velocity difference between the whisker and the vortex-induced velocity field. The second was the pressure component, which arose from the influence of the pressure-field surrounding the vortex core on the whisker, and the result of which is a notable 'jerk-like' response in the motion of the whiskers (Muthuramalingam & Brücker 2019). This type of temporal response on the passing-by of turbulent structures can be beneficial to conditioning the original signals to achieve higher accuracy of the CC but which is not necessarily required.

Whiskers

The focus of this study has been to test the effectiveness of the design and thus the functionality of FBG-based optical whisker sensors, comparing their performance against the previously-used optical whiskers (Muthuramalingam & Brücker 2019, Glick et al. 2021, 2022) which were tracked using a camera with integrated tracking software. Here the aim was to explore the benefit of the FBG-based whisker approach to monitor the outer flow field from inside the body from which the whiskers protrude. The setup used in this investigation (see fig.4.4) reflects the needs of this study, where all the whiskers protrude from a flat plate, normal to the plate, and are spaced at regular intervals. All the forces and the motion above the plate were negated by clamping the whiskers at regular intervals above the plate and fixing them to the plate where they pass through small holes drilled into the plate. Therefore it was only that part of the sensor that protruded below the plate that responds to the flow. Further and irrespective of the material used, the whisker-like fibres acted as cantilever beams, clamped at the root, free at the end, and which deflected according to the velocity-related drag force and the force due to the pressure-field induced by the vortex. Those forces changed over time when the vortices pass each sensor.

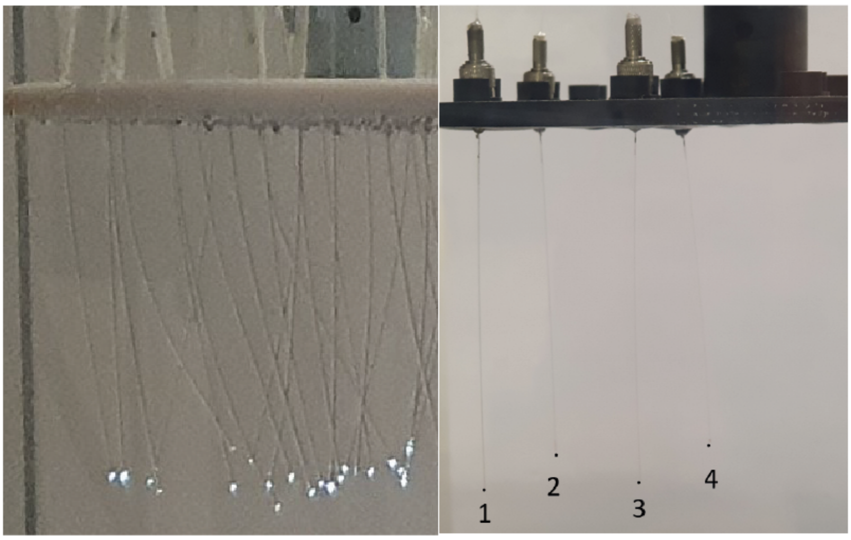

Figure 4.2: Left: Plastic fibre array under disturbance from a vortex ring moving from left to right. Right: Close-up view of the glass fibre array in similar scale and position.

In this study, the performance of the originally-used artificial whiskers, made of 750 µm transparent polymer fibres, was taken as the 'baseline' from which the enhanced performance of the new FBG-based silica fibre sensors, designed and evaluated in this work, could be assessed. The polymer fibres were bundled together and illuminated from one end with an LED light source. The light exits at the other end, illuminating the whisker tips. The position of the whisker tip light spots was tracked by a high-speed tracking camera (as shown in fig. 4.1). The polymer fibres used were 80 mm in length and 750 µm in diameter, and were arranged in a five-branch spiral array with logarithmic spacing. The design developed has been based on the key features of designs for aero-acoustic microphone arrays, which seek to minimise co-linearity for better beamforming performance (Arcondoulis et al. 2011). Despite how closely packed the fibres appeared (as visible in fig. 4.2), they were out of plane from one another, positioned roughly 0.35 whisker lengths apart.

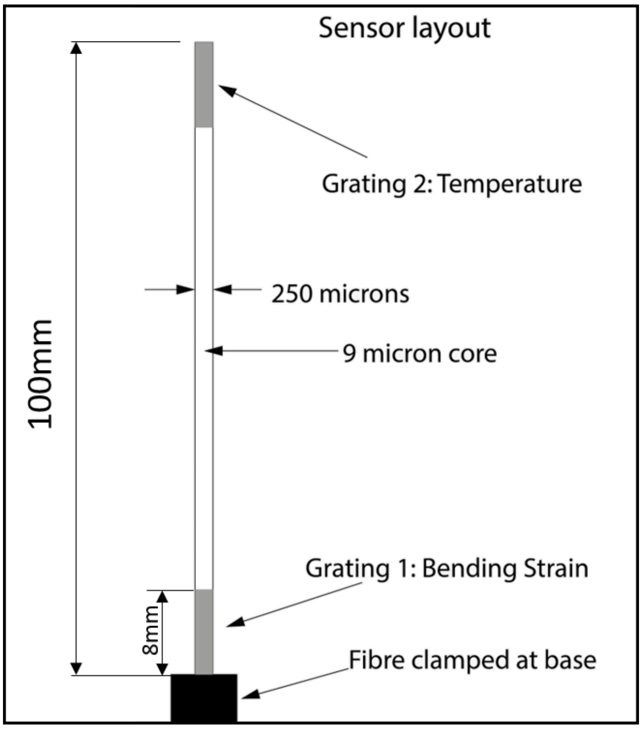

Figure 4.3: Diagram of a silica optical fibre sensor. The oscillations at the sensor's eigenfrequency dominate the sensor's response to excitation in air, but are heavily damped when underwater.

Further, due to the intentionally irregular layout of the array, at any given DoA there were only a few whiskers directly in the wake of another whisker closer than 0.6 whisker lengths, reducing the prominence of Vortex Induced Vibrations (VIV). The silica sensors used were 80 mm long and were made from 250 µm diameter optical fibres, (with a 9 µm core diameter). The smaller diameter and different materials used mean that the silica fibres have lower bending resistance than the polymer fibres. On the other hand, they also have a smaller frontal area which results in lower drag force. Both effects combined resulted in a similar order of tip displacement magnitudes to the polymer fibres when observed under similar flow conditions. The key feature of the silica fibres was the set of FBGs written into them to act as strain and stress sensors. The fibres thus had an 8 mm long grating written at the root of the fibre, just beyond the clamping point, and were designed to be where the bending was concentrated, see fig.4.3. Ordinarily, such fibres are most sensitive to axial loads and typically not very sensitive to bending. However, ensuring that the gratings used were positioned at the site of the most concentrated bending forces which maximises the sensitivity of the fibres to the bending forces. This consistently produces a measurable wavelength shift. It can be noted that temperature sensitivity is a useful secondary function of the FBG sensors (when used as temperature sensors (Pal et al. 2004), but this means that the gratings are very sensitive to temperature fluctuations including when the measurement of any other parameter is required. To deal with this problem, an approach used in several other sensors by some of the authors (Rente et al. 2021) has been employed where a second (in this case strain relieved) grating is used to monitor any temperature fluctuations on their own. This way, the sensor system could differentiate the wavelength fluctuations due to bending alone, with this second grating placed on the sensor, away from the root, and towards the tip (where the bending forces are much weaker and thus temperature is the primary measurand).

This approach was used to normalise the root sensor output and thus deal with any potential interference in the measurement from any fluctuations in temperature. This was particularly important for field applications, especially in situations involving the mixing of two or more flows at different temperatures. The fibres used were glued into SMA connectors that were designed to slot into sockets built into the 3D printed plate (and visible in fig.4.2). The change in the wavelengths of the FBGs written into the fibres were monitored using a commercial FBG interrogator, (type Micron Optics sm130), which was used to track the shift in wavelength of the backscattered light from the FBG sensors, at a maximum sampling rate of 2 kHz (which was more than adequate for the work carried out). The FBG wavelength used was 1536 nm (chosen to match the spectral output of the interrogator) at 10 °C and in use showing maximum variations of less than 1 nm. The FBG sensors written into the fibres had a reflectivity of 60%, and had a bandwidth of 250 pm.

Calculation of the Cross Correlation & Direction of Arrival

The calculations used herein follow the same method as used for the post-processing of the tip-displacement signals from the polymer fibres in our previous work (Glick

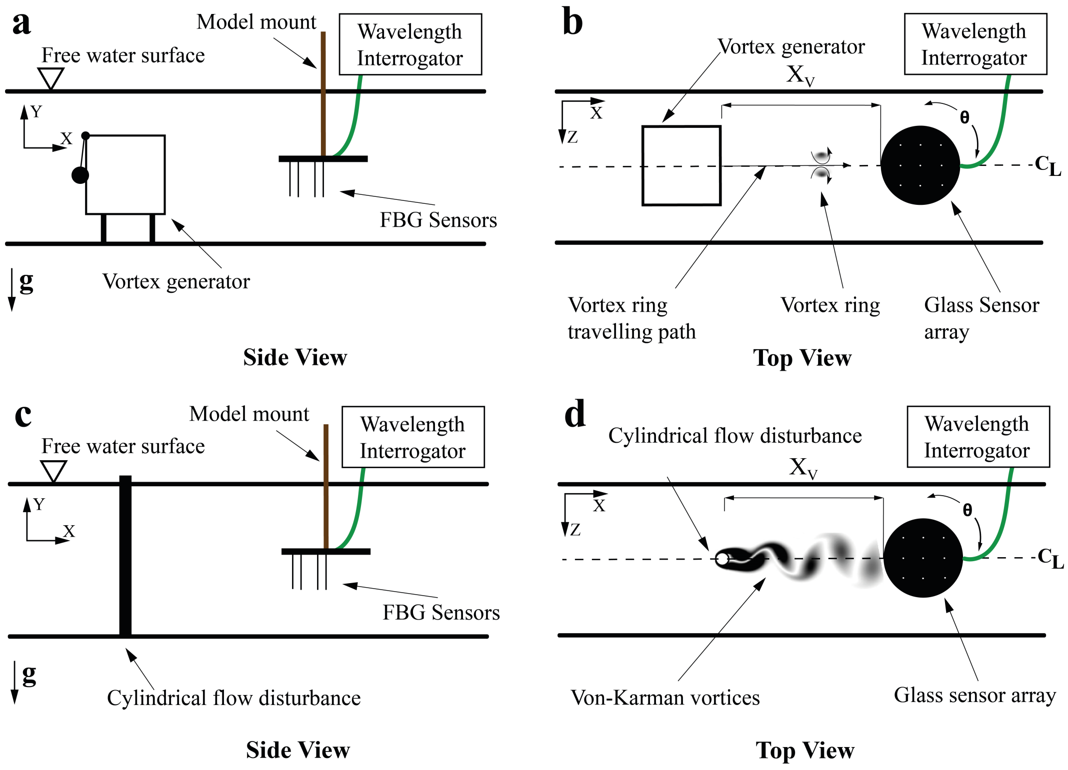

Figure 4.4: (a-b) Schematic diagram of the whisker array and vortex cannon, shown here with the FBG sensors. The setup is the same for the plastic fibre arrays but with the addition of the tracking camera as pictured in fig.4.1 (c-d) Setup showing the cylinder upstream of the array. For both setups, the disturbance source remains stationary but the array is rotated about its centre.

et al. 2022) (See Appendix A for more information). In the case of the FBG-based whisker sensors, the bending-related frequency shift signal was processed by the Micron Optics interrogator and transformed into a digital output at 2kHz. The method of temporal cross-correlation of the output between triplets of whiskers was used to generate the TDOA information for each whisker in the array, with the same basic Generalised Cross Correlation (GCC) algorithm (Knapp 1976) as described in our previous work (Glick et al. 2022). A minor improvement to the code was implemented through the addition of a pre-CC filter that removed any undisturbed or seemingly anomalous sensor outputs and which then places less emphasis on the signals from whiskers experiencing a smaller deflection. This approach was implemented in this work, due to the much larger arrays used in the final part of the study described. It was noted that attempting to use all the sensors in the larger arrays yielded little to no improvement to the information received but had the penalty of raising the computational times very significantly. The subsequent DoA calculations undertaken also used the same method of multilateration based on acoustic source localisation techniques (Ollivier et al. 2019). Herein the known spacing between the fibres at their roots was provided as an input into the calculations.

4.4 Results of the Investigation

Sensor performance

In this study, the key information required is on the performance of the sensors and thus to verify the improvement in performance due to the new FBG-based whiskers employed. The important metrics which were used to characterize the performance of the sensors studied were as follows: sensitivity – thus the weakest signal that can be seen when a single sensor was deflected to the minimum perceivable point; the Signal-to-Noise Ratio (SNR) of the output signal; and the presence of Whisker Induced Vibrations (WIV) or Vortex Induced Vibrations (VIV) in the signal observed. The performance of the DoA algorithm used has already been assessed in a previous paper (Glick et al. 2022), (and thus this is not reproduced here), although the specific physical factors that influence that performance, including sensor length, spacing, and eigenfrequency, are briefly discussed below, for completeness. The absolute sensitivity of the sensors developed is known to depend heavily on the source of excitation. For the purpose of this study, the reasonable assumption was made that this was a vertical vortex roller, carried with the flowing water, and hitting the length of the vertically arranged whiskers evenly. For flow speeds below 5 cm/s and at cylinder distances larger than 10Dc the roller did not have enough energy to deflect the sensor sufficiently to be perceived from the output signal against the background noise. This can be regarded as the resolution limit of the FBG whiskers in the current study.

The SNR of the FBG fibres was calculated from the magnitude of the shift in the wavelength of the back-scattered light while deflected compared to the maximum fluctuations in wavelength due to background noise. In comparison, the SNR of the polymer fibres was calculated from the magnitude of deflection when disturbed compared to the maximum variation in position in undisturbed flow. The overall performance of the sensors (in terms of the SNR) under the same excitation conditions can be seen in fig.4.5, with the SNR of the polymer fibres used for comparison with the performance of the FBG-based sensors (see fig.4.9 for sensor deflection characteristics). Here what can be clearly seen was the increase of SNR

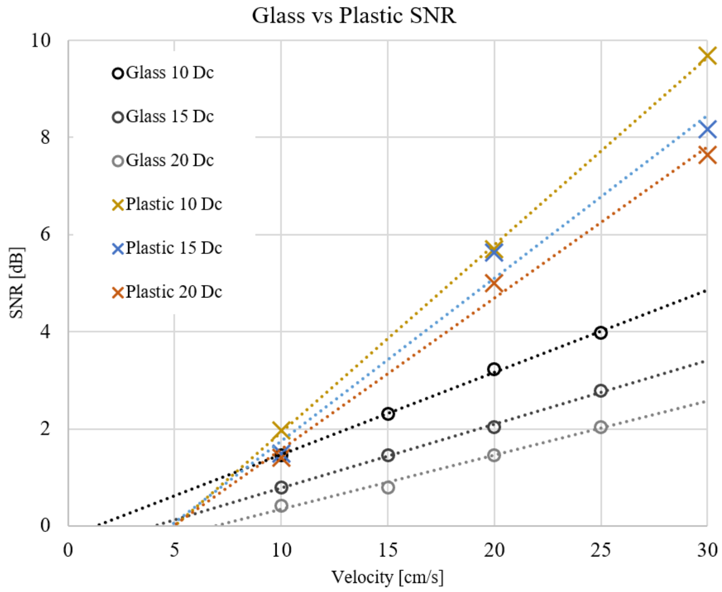

Figure 4.5: The sensors were disturbed by a series of vertical vortex rollers passing by, shedding from the cylinder placed upstream of the array, and carried with the flowing water. The rollers hit the length of the sensor evenly. This signal was chosen for comparison as it is the weaker of the two signals discussed herein.

with increasing speed of the mean flow, which is related to the stronger forces (mean and fluctuating) imposed on the whiskers. The laboratory situation used for these tests provided the optimal conditions for evaluation of the performance of both the (FBG-based) silica and the polymer fibre sensors, where it can be seen that the polymer sensors outperform the silica sensors. However, in the 'real world', the field conditions experienced worsen the performance of the visually tracked systems (the polymer fibres) due to the presence of interference from vibrations, ambient light, and likely sub-optimal camera placement. By comparison, the SNR of the silica (FBG-based) fibres is still large enough for the calculation of the CC and DoA, where the performance is discussed below (and shown schematically in fig.4.6).

An approach to improving the SNR by filtering out some of the noise was taken by employing a wavelet domain reconstruction of the signal. This was found to offer a small improvement in the quality of the CC, but at the cost of a notable increase in computation time, making it a valuable addition for applications that are not time sensitive.

Estimation of the DOA Performance

There are two metrics for the evaluation of the DOA performance of the whisker sensors developed in this work. The first is the prediction trend line, where the trend line gave an overall estimation of the accuracy of the prediction, and its gradient indicated a preference or skew towards an over or under-prediction of the direction of arrival. The distance between the intercept on the y-axis and the origin indicates any degree of angular skew present. The second metric used is the Root Mean Squared Error (RMSE) of the set of predictions, measured across the range of angles tested. In this work, repeat readings generating multiple signals could be used to improve the accuracy of the results obtained, but to do so requires repeat observations of the same source, from the same position. However, in both nature and many of the in-the-field application scenarios, the source of the disturbance would be moving, and so the occurrence of such a scenario was unlikely. Therefore, in this work, the RMSE of the sensors was calculated using single flow disturbance events. The results of such an investigation were encouraging, as overall, the prediction of the performance was very good, so long as the signal strength is sufficient to create a well-populated TDOA matrix. As the distance to the source increases, the gradient of the trend-line drops slightly, this being possibly due to the rate at which the disturbance is slowing down. The intercepts for all graphs examined were within a few degrees of the origin, indicative of a small overall skew, but giving a result which is within an acceptable range, given the typical RMSE data set of around 3.5°. The performance of the silica (FBG-based) sensors was compared to that of the polymer sensors, at distances of 200 mm and 300 mm (as can be seen in fig.4.8). It is evident that the performance of the polymer grid array was worse than that of the silica fibres, at both distances, by about 20% with the RMSE obtained being typically around 4.2°. The similarity of the goal of the most effective use of the sensors to other applications was noted, which lead to the final outcome of the study. In order to verify the impact of highly co-linear arrays on the predicted performance, a polymer fibre spiral array design (as described above) was used to capture potential performance improvements, aimed to be translated to a larger array of silica sensors. As expected, the spiral array showed a marked improvement compared to both grid arrays, with a typical RMSE of just 1.9° as shown in fig.4.7.

Computational savings

Finally, the computational savings associated with the simpler output of the new FBG-based sensor system were evaluated. When comparing the time taken to calculate the DoA it must be noted that the polymer array is larger and therefore has

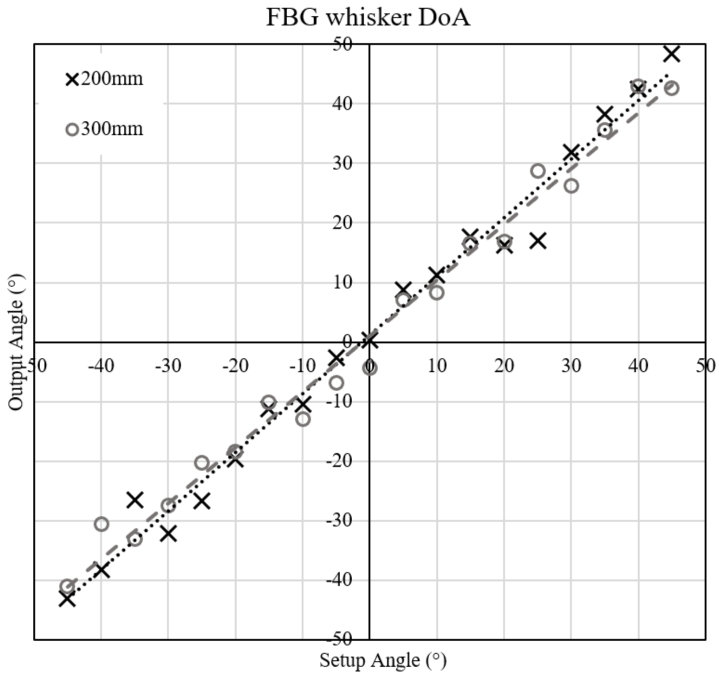

Figure 4.6: Performance deteriorates slightly with distance to the source. The performance at 200-300mm is still excellent with RMSE of 3.5° and 3.7° respectively

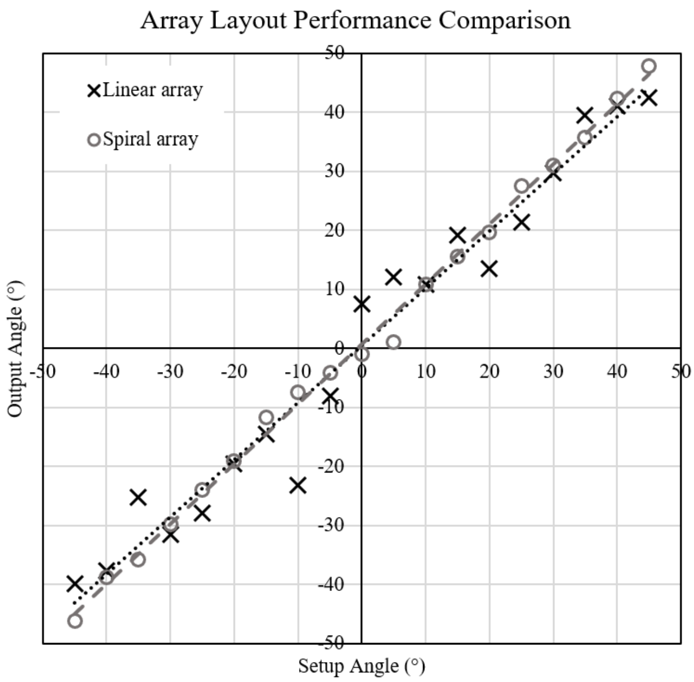

Figure 4.7: Arrays spaced 200 mm from the source, with the same inter-sensor spacing.

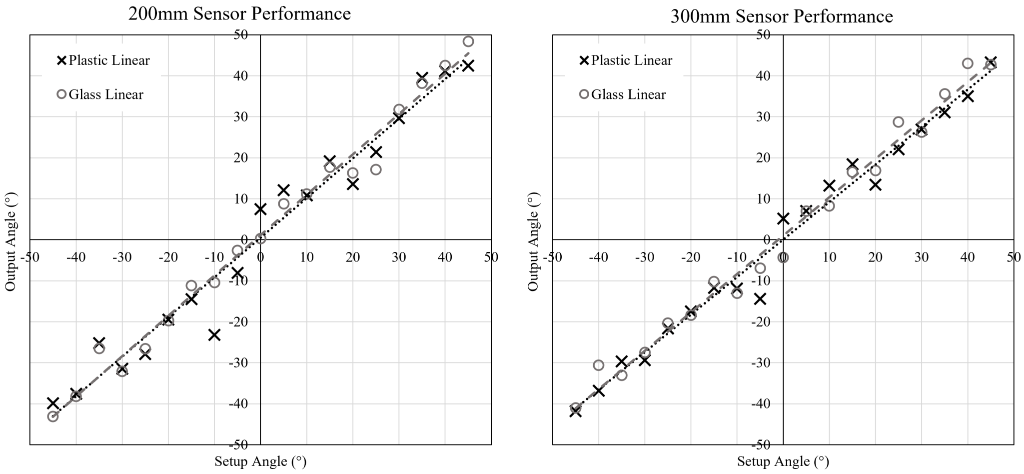

Figure 4.8: Array layouts performance assessed using large numbers of visually tracked plastic sensors spaced 200 mm from the disturbance. This spiral array is inspired by similar array designs for acoustic microphone arrays, used for acoustic source localisation(Arcondoulis et al. 2011)

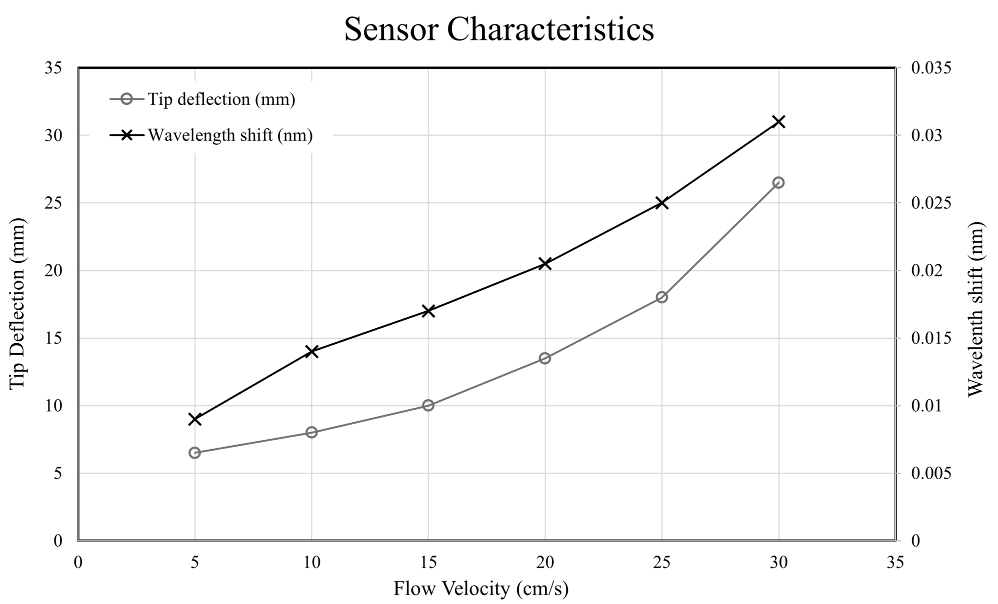

Figure 4.9: Sensor performance in turbulent flow. The array of sensors can function provided the magnitude of the wavelength shift is sufficient to allow for reliable inter-sensor CC, (around 0.012 nm given present noise levels of ±0.006 nm).

more sensors to track, evaluate, select from, and then on which to perform the cross correlation. Taking all this into account, the polymer fibres rely on the use of a tracking camera, the output of which requires extra steps to create the sensor tip displacement track, resulting in a like-for-like time save compared to the silica fibre, FBG-based sensors, of around 40%. This number does not account for the internal processing time of the tracking camera or the FBG interrogator (tracking the shift in wavelength of the FBG sensors), but conveniently the delay from both of these components was extremely small and could be ignored, compared to the DoA computation time. Given the value of real-time direction tracking, these improvements were significant, and with a more powerful system could potentially realize a delay of only a couple seconds which would be acceptable for most industrial applications.

4.5 Discussion

The data from the investigation has shown that the square arrangement of the four FBG-based sensors in the silica fibre offered a real performance improvement over the larger, grid array of polymer sensors, even though the individual SNR figures for these sensors were somewhat poorer than those of the sensors in the polymer fibre. This result was obtained for the investigation carried out under laboratory conditions, but it can be noted that the FBG-based sensors will perform better in the field, due to the different scaling factor of the size of the disturbance (the vortex diameter), relative to the spacing between the fibres in the two different arrays. When evaluating the silica sensors, the array and disturbance source were carefully aligned such that all four sensors would fully experience the effect of the disturbance each time. For the larger 2D array, the significant co-linearity of the array may have made several of the disturbed whiskers redundant. A potential way to overcome this effect is to use an array with non-linear spacing such as in the spiral arrangement, also commonly employed in audio-cameras when using beamforming reconstruction algorithms for source localization. As can be seen from fig.4.6, the further the array is positioned from the disturbance, the shallower the gradient of the trend line, i.e. the tendency is then to a potential underestimation of the angle to the disturbance. This effect is expected as the vorticity field dissipates with the distance travelled from the source and therefore the energy of the disturbance exciting the sensors decreases and approaches at some distance the noise level experienced for an individual whisker.

The SNR of the FBG-based sensors written into the silica fibres due to the imposed bending stress from the flow-induced forces overall is at a low level, indicating that this alone cannot be a sufficient indicator of flow speed or direction. However, as the correlation principle of temporal differences in the response of fibres in the array is being used, the convection velocity at which the disturbance travels and the direction from where it hits the array can be calculated. Therefore, under the conditions presented herein, and using the methods as described above to process the signals, the data were sufficient to track the source's disturbances. Under less favourable conditions, or when facing weaker stimuli, a higher SNR would likely be preferable. In order to track a single source when multiple sources are present, i.e. in an environment with higher background noise, a greater sensitivity would be preferable. To achieve this, further work could be done on mechanical changes to the whisker size and strength to optimize these to enable adjusting the minimum required force on the sensor to be greater or smaller as needed.

In this research, fibres of a core diameter of 4 µm were tried first, but these did not produce sufficient wavelength shift under deflection. Fortunately, alternatives are available and so FBGs were written into larger core (9 µm) fibres, and these were found to give sufficient compression/expansion of the FBG and resultant change in wavelength. Contrary to conventional usage, under bending stress, a wider core results in a larger wavelength shift. The wider core results in the outer section of the fibre core being subject to greater strain due to the cross-sectional load concentration of a beam under bending stress, resulting in a larger wavelength shift.

There is further scope for enhancing the sensor performance by making changes to the whisker profile and cross-section as this could alter the drag force at a given flow velocity, thus changing the threshold flow speed at which the whisker starts moving (and thus this can be detected). Further enhancement of the system could be achieved by stiffening the fibres (apart from at the root), as this could offer potential improvements to the SNR by capturing more of the bending motion occurring at the root of the fibre (where the FBG is positioned), rather than allowing the typical bending profile of a uniform beam where some of the bending would occur along the length of the beam.

The main limitation of such an approach is to avoid the sensors becoming overly sensitive to shocks and knocks (and thus require more protection with additional coating). A downside of such an approach is that the stiffness created in the fibre may then counteract any additional sensitivity gains. The process used to re-apply the polymer coating to the engraved optical fibres could have also contributed to a decrease in the sensitivity of the whiskers (as the writing of the FBGs in the fibre requires the removal of the primary coating, which is then reapplied to protect the fibre). The re-coated sensor's polymer coating was slightly thicker than the original coating (by about 20-30 µm). This thicker coating was located inevitably at the position of written FBG, thus with a potential impact on sensitivity. A further minor issue is that the wider re-coated fibre root did not fit exactly into the standard-sized fibre SMA connectors which were used to secure the fibre and therefore a larger connector had to be used, with the fibres glued in place. Unfortunately, this larger orifice still did not clamp the fibre perfectly, which could have let the fibre deflect a little behind the clamping point, thereby reducing the bending at the grating, and therefore the sensitivity of the sensor.

The above points to several of the potential enhancements to the system that could be implemented in future work, building on the success of the results obtained from this investigation.

4.6 Conclusions

The work done has been innovative in its approach, using FBGs written into silica fibre, to create a very effective means of tracking hydrodynamic disturbances with fibre optic whiskers. The study carried out has shown that such an array of FBG sensors can produce very good estimations of the velocity and DoA of flow disturbances which pass the sensors. An important feature of the design is that a small number of fibres are used, offering high-quality, reliable and rapid measurement with an array consisting of only 4 sensors (in a grid arrangement). The results obtained have demonstrated the precision of the measurements made, based on the principle described, showing that it would be possible to build an effective array of this type of FBG-based whisker sensors mounted on unmanned underwater vehicles to track passing objects. As demonstrated with a larger array, it is easy to increase the number of sensors (by simply adding more FBGs written at different wavelengths into the fibres, as the Micron Optics interrogator used has considerable scope for detecting over a wider bandwidth), offering an improved layout which can further improve the DoA estimates. Thus in further work, scaling up the array is a key target.

In this research, methods to increase the potential precision were tested and show some promising trends. Furthermore, machine learning is a valuable tool that could be brought to bear on this problem and thus could potentially improve signal tracing, allowing for better performance at lower SNR, or offering valuable SNR enhancement. Supporting this, Elshalakani et al.(Elshalakani et al. 2020) have demonstrated that machine learning can make good predictions in whisker systems, based on RMS values of the bending magnitude. There is therefore good reason to suggest that it could do the same with time-domain based DoA estimations helping with filtering, or processing the signal at various stages of operation. Thus there is considerable scope for enhancing the performance of the system in the ongoing research into this interesting phenomenon.

4.7 Appendix A: Direction of Arrival Calculations

The Direction of Arrival is defined as the angle between the oncoming vortex ring and the anteroposterior axis of the model, in the horizontal plane. The bow-wake effect of the travelling vortex ring is causing the initial deflection of the whiskers and is approximated across small distances as a signal propagating with a planar wavefront.

The inputs to the multilateration function are the arrays of time delays between every pair of whiskers, and the X and Y position of each whisker tip while the whisker is at rest. The time delays are calculated via a Generalised Cross Correlation function (Knapp 1976), as a function of the whiskers displacement.

The calculation relies on the basic principle of TDOA multilateration. It differs from other conventional use cases in that both the time of the signal's emission and the speed of the signal are unknown. To account for this, triplets of sensors are used instead of pairs that are typically used when the speed of the signal, or the signal emission time are known. This allows for the calculation of the DoA by comparing the ratio of the TDOA with the ratio of the distance between the sensors, a comparison that is independent of the signal's velocity or time of emission.

Assuming that the direction and velocity of the signal remain constant when travelling over the triplets, looking at the time difference between the excitation of three whiskers of known positions should produce the angle and velocity of the signal as follows:

$$\frac{\Delta T_{AB}}{\Delta T_{BC}} = \frac{L_{AB}(\gamma)}{L_{BC}(\gamma)} \tag{4.1}$$

where 'ΔT' is the time difference between the whiskers A and B, and 'L' is the distance between points A and B in the direction of travel, (γ).

$$L_{AB}(\gamma) = cos(\Theta_{AB})\sqrt{(x_B - x_A)^2 + (z_B - z_A)^2} \tag{4.2}$$

The coordinates 'x' and 'z' represent the pixel positions of whisker tips A and B, and Θ_{AB} is the angle between $L_{AB}(\gamma)$ and the line AB:

$$\Theta_{AB} = 180 - \gamma - \alpha_{AB} \tag{4.3}$$

where 'α_{AB}' is the angle between the distance vector $\vec{AB}$ and the z-axis, and 'γ' is the angle of the propagating signal front.

To find the solution, an algorithm is applied that scans all possible values of γ, from -90 to 90 degrees in 0.002-degree increments, recording the range of values of γ that satisfy equation 3.4 to four significant figures. The size of the range of resulting values provides an estimate of the uncertainty in the angle output of that whisker triplet and is mostly dominated by the size of γ, as small angles result in small time delays between whiskers in the triplet, which are therefore more sensitive to random error. This is repeated for all viable triplets of whiskers (With low co-linearity and sufficient deflection), and the result is taken from the displacement-weighted average of the γ outputs:

$$\bar{\gamma} = \frac{\sum_{n=1}^{m}(\gamma_m * \frac{MinD}{\bar{D}})}{m} \tag{4.4}$$

where 'MinD' is the minimum displacement of any whisker in the triplet, and '$\bar{D}$' is the average whisker displacement across all measurements.
The travel velocity of the signal is therefore simply estimated as:

$$\hat{V}_s = \frac{\sum_{n=2}^{p}\frac{L_{1,n}(\bar{\gamma})}{\Delta T_{1,n}}}{p-1} \tag{4.5}$$

where $L_{1,n}(\bar{\gamma})$ is the length between points 1 and n, at the calculated $\bar{\gamma}$, and $\Delta T_{1,n}$ is the corresponding time delay. Error in the travel velocity due to recorded vertical variation in vortex exit angles ($\pm 2.7^{\circ}$) is calculated as follows:

$$\%Error = \frac{\hat{V}_s - \hat{V}_s * Cos(2.7^{\circ})}{\hat{V}_s * Cos(2.7^{\circ})} * 100 \tag{4.6}$$

The lowest recorded velocities were roughly 1 m/s, leading to a maximum error of 0.11%.

4.8 Critical Analysis

4.8.1 Characteristic response of fibre optic whiskers in air

This section details an early study into the viability and best design principles of the glass fibre optic sensors. This study observed the behaviour and response of glass fibre optic sensors in air, under disturbance loads (gusts) generated by compressed air, fired past the sensors. Describing the response of glass fibres in air did not require a large array, so for simplicity, this test was carried out in 1D, with two sensors in line with the direction of flow.

Unlike several of the setups used above, This setup 4.10 had the sensors supported at the base, with the fibre protruding upwards. The sensors were spaced 200mm away from the nozzle, as in the water tunnel, but on a sliding jig, that allowed for the distance between the sensors to be adjusted. This was used to take a series of measurements at progressively shorter spacings, enabling us to evaluate the impact that WIVs have on a sensor's response in air.

Also differing from other setups was the temperature difference between the ambient and the flow disturbance. The compressed air jet is about 20°C colder than the ambient, and is a fairly narrow jet. As discussed above, the sensors are fitted with strain-isolated temperature gratings, to offset fluctuations in the strain grating sensor output due to temperature changes in the fluid. These worked as intended here, but highlighted a slight weakness of the design when used to monitor flow mixing events with a large temperature difference between flows. In situations like this the distance between the gratings on the sensor could lead to an under or over representation of temperature effects. This is of limited concern as the sensors are unlikely to operate in such conditions when used to monitor motion in large bodies of water, that generally have very consistent ambient temperatures (Ptak et al. 2016, Hannah & Garner 2015), often year round.

At 7m/s, the airflow has a similar whisker diameter based Reynolds number ($Re_{Dair} = 130$) to the water setup ($Re_{Dwater} = 210$). One of the key differences between the air and water tests is the vibration response of the whiskers. In water the sensors are heavily damped, but in air multiple vibration modes are present, based on the Eigen frequency of the fibre, and the VIV frequency of the shed vortices. This response highlights the impact of water's damping effect on the sensor response while submerged. While this setup exacerbated the Eigen frequency mode due to the

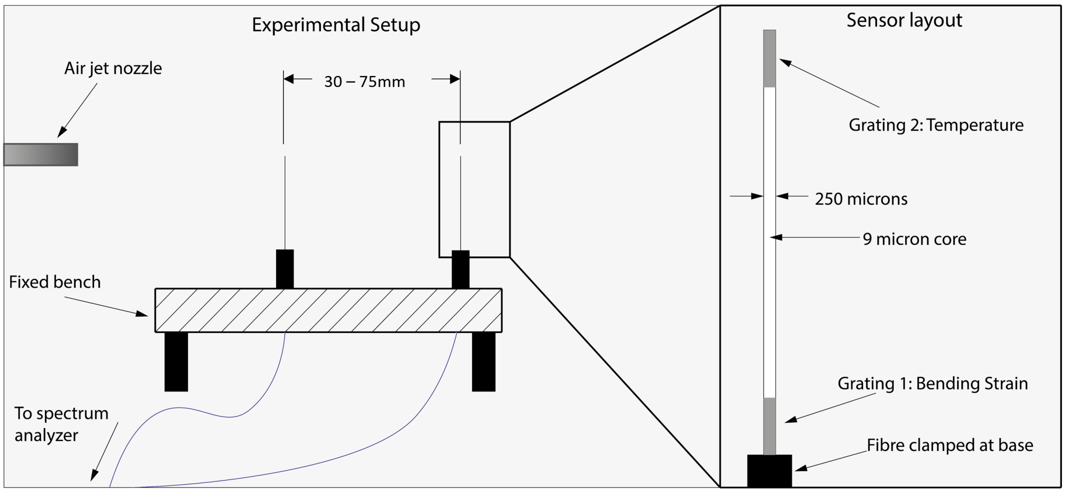

Figure 4.10: Compressed air jet fires with an initial velocity of 7 m/s, and whiskers are 80mm long

orientation of the fibre, the fibres low mass does reduce this effect. When hanging from the clamped point the fibre is stable in its 'neutral' position, but positioning the fibre's centre of mass above the clamped point introduces an instability that keeps the fibre oscillating for slightly longer. This impacted the quality of the cross correlation when using time windows close to the period of vibration. For computational reasons it was decided to use time windows that were sorter rather than time windows that could capture the full profile of the vibration.

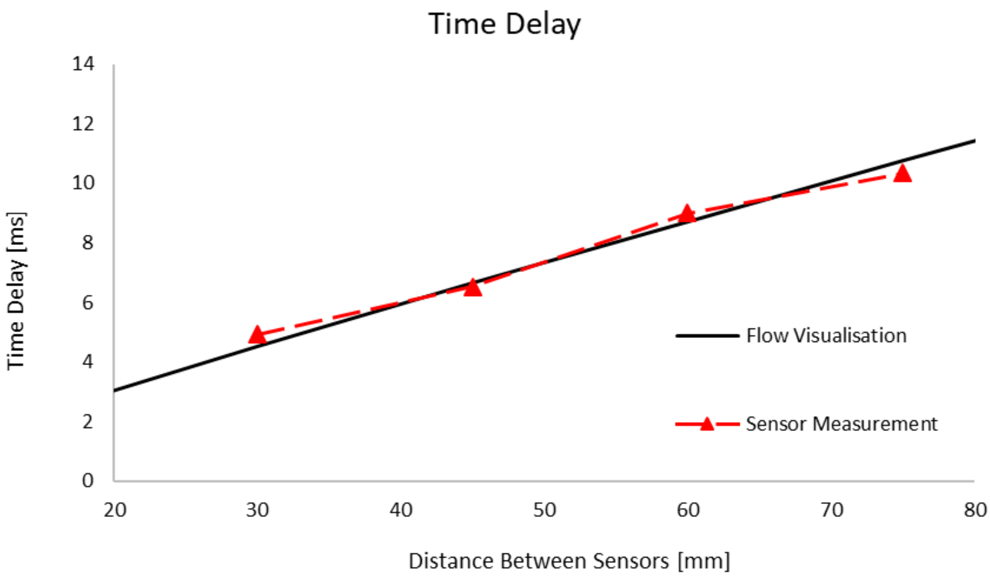

Figure 4.11: Measured flow rate at the sensors is approximately 6.5m/s

The time delays recorded by the sensors (as shown in: 4.11) produce velocity estimates that are in line with measurements taken using high speed Schlieren imaging recordings of the compressed air flow leaving the nozzle. This built confidence in the sensors ability to be used for multilateration applications in air, despite the minimum airspeed requirements for detection being high enough to limit the scope of some applications (approx. 3-4m.s). It was noted that due to the weak effects of WIVs, and the strong vibration of the whiskers, whisker spacing had negligible impact on the sensor's response, even when spaced at just 0.3 whisker lengths apart. This informed the design of future arrays, giving confidence that whisker spacings of 0.4-0.5 whisker lengths would not cause excessive WIVs.

General questions raised by reviewers

1. **Given that generally, a thinner fibre has a higher stress or strain response, how does a 9µm core fibre produce sufficient wavelength shift under deflection, but the narrower 4µm core fibre does not.**

   Unlike FBG sensors used to detect axial stresses, when under bending stress a wider core results in a larger wavelength shift. This is due to the cross-sectional load concentration of a beam under bending stress, where the outer most section of the fibre core is subjected to the greatest stress. Therefore a wider core diameter sensor experiences greater strain which results in a larger wavelength shift.

2. **To what degree would a different medium affect the experimental results?**

   The sensors used in this work were designed for and used for measurements in water. Despite this, the versatility of our time based approach means that, without altering the sensors, a fairly wide range of mediums could be used without suffering significant performance losses. The sensors rely on tracking the time signatures of convected flow effects, and therefore altering the specific bending response of the sensor, due to viscosity or mass density of different fluids, would not prevent the sensors from producing accurate results when measuring flow speed. This is because the measurand is not the magnitude of the sensor displacement, but the time delay between two or more sensors placed a fixed distance apart.

   Having said that, the range of flow speeds that the sensors perform well in, and the maximum flow speeds they can be exposed to without sustaining damage, will vary with the density of the medium used. We carried out a study on an early version of the sensors, assessing their performance in air (see Thesis Appendix A), and found that the sensors could track disturbances in air provided the flow speeds were high enough (approx. 3m/s). The sensors were much noisier in air as they vibrated for much longer due to the reduced dampening effect of the lower viscosity medium. This degraded the sensor performance at low flow speeds, where the smaller deflections were harder to detect. If the sensors were to be used in a glycerine mixture then the minimum and maximum operating speeds would be lower. While the heavier dampening might reduce the noise further, it is unlikely to change the results much overall.

3. **How would the sensing curves of wavelength shift and tip deflection as a function of flow rate change with medium**

   Sensing curves representing wavelength shift as functions of flow rate have been included in the paper. One of the benefits of the sensor system we present in this paper is that the individual sensors do not need to be calibrated. The specific wavelength shift is unimportant to our sensors and sensing system, that simply report when they have been disturbed. By communicating this time delay of arrival across the array of sensors, we can find the flow velocity.

   Nonetheless, the patterns exhibited by the sensing curves are as expected for small deflections. Tip deflection scales linearly with drag force, which in turn scales as a function of the velocity squared, aligning nicely with the drag equation. Wavelength shift is a product of the deflection angle, but with a dead zone at small angles of deflection which is what gives rise to the minimum detectable flow velocity of 5cm/s as below that the wavelength shift is less than the fibres' background noise level of roughly ± 0.005nm (for reference see fig.4.9).

Future work

The results from these studies forms a performance baseline which can inform the design of further iterations of accurate and robust sensors. The first area of further investigation is the tracking of out of plane motion. The style of arrays presented can be used to investigate out of plane motions by considering the rarefaction and compression of the average whisker tip position. The transition to FBG sensors made this more difficult than with previous arrangements due to the small number of sensors, and the "blind" nature of the setup. The system is "blind" as whiskers are known to have deflected but not the direction in which they have moved. The performance of this could be investigated with additional sensors. The subtraction of mean flow from the whiskers motion, and with sufficient data, the subtraction of motion due to specific disturbances, would in theory leave only turbulence, and the motion due to out of plane effects. This could allow for detection of the centre of rarefaction, and subsequently the speed and angle of the out of plane motion.

The next logical stage to this research is preparing for in situ measurements. This would involve developing fibre coatings to ensure that the fibres can operate without sustaining damage, while still detecting the forces at the desired tracking window for objects within a target size bracket and range of speeds. This is a materials problem which would need to be catered to the targeted deployment environment (i.e. freshwater, saltwater, wastewater, etc.) and the chemical or mechanical challenges posed by each.

There is also interest in studying the neuro-processing of pinnipeds and other whiskered animals directly. There is much scope for studying the way that pinnipeds' brains process this information naturally, be it using left vs right comparison, correlation between stimulated whiskers, or perhaps in a method more similar to the neural delay lines common in schools of fish swimming together. such a study could also further investigate the use of the animals various senses, and which they rely on most heavily, be it auditory, tactile, or as in this research, the time components of the whiskers' motions. This could inform the design of hybrid artificial systems that seek to blend multiple processing methods into increasingly accurate methods of DoA flow monitoring.

Bibliography

Adachi, T. et al. (2022), ‘Whiskers as hydrodynamic prey sensors in foraging seals’, *Proceedings of the National Academy of Sciences* **119**(25), e2119502119.

ANSYS (2019), *Ansys Fluent Tutorial Guide*, ANSYS.

Arcondoulis, E., Doolan, C., Brooks, L. & Zander, A. (2011), A modification to logarithmic spiral beamforming arrays for aeroacoustic applications, *in* ‘17th AIAA/CEAS Aeroacoustics Conference (32nd AIAA Aeroacoustics Conference)’, pp. 1–12.

Axtmann, G., Hegner, F., Brücker, C. & Rist, U. (2016), ‘Investigation and prediction of the bending of single and tandem pillars in a laminar cross flow’, *J Fluids Struct* **66**, 110–126.

Barth, F., Humphrey, J. & Secomb, T. (2003), *Sensors and sensing in biology and engineering*, Springer-Verlag Wien, New York.

Bearman, P. (1984), ‘Vortex shedding from oscillating bluff bodies’, *Ann. Rev. Fluid Mech.* **16**, 195–222.

Bleckmann, H. & Zelick, R. (2009), ‘Lateral line system of fish’, *Integrative Zoology* **4**(1), 13–25.

Blevins, R. (1990), *Flow-Induced Vibration*, Van Nostrand Reinhold Company, New York.

Bodaghi, D., Wang, Y., Liu, G., Liu, D., Xue, Q. & Zheng, X. (2023), ‘Deciphering the connection between upstream obstacles, wake structures, and root signals in seal whisker array sensing using interpretable neural networks.’, *Front Robot AI.* **10**(1231715).

Bruecker, C. (2016), 'Measurement of near-wall 3d flow velocity from wave-guiding micro-pillars', *Opt. Express* **24**(19), 21407–21414.

Brücker, C., Bauer, D. & Chaves, H. (2007), 'Dynamic response of micro-pillar sensors measuring fluctuating wall-shear-stress', *Exp Fluids* **42**, 737–749.

Brücker, C. & Rist, U. (2014), *Complex Flow Detection by Fast Processing of Sensory Hair Arrays*, Springer, Berlin, Heidelberg.

Brücker, C., Spatz, J. & Schroder, W. (2005), 'Feasibility study of wall shear stress imaging using microstructured surfaces with flexible micropillars', *Exp Fluids* **39**, 464–474.

Chagnaud, B., Brücker, C., Hofmann, M. & Bleckmann, H. (2008), 'Measuring flow velocity and flow direction by spatial and temporal analysis of flow fluctuations', *J. Neurosci* **28(17)**, 4479–4487.

Deer, W. & Pounds, P. (2019), 'Lightweight whiskers for contact, pre-contact, and fluid velocity sensing', *IEEE Robot. Autom. Lett.* **4(2)**, 1978–1984.

Dehnhardt, G., Mauck, B. & Bleckmann, H. (1998), 'Seal whiskers detect water movements', *Nature* **394**, 235–236.

DeRuiter, S. et al. (2013), 'First direct measurements of behavioural responses by cuvier's beaked whales to mid-frequency active sonar', *Biol. Lett* **9**(20130223).

Dolman, S., Evans, P., Notarbartolo-di Sciara, G. & Frisch, H. (2011), 'Active sonar, beaked whales and european regional policy,', *Marine Pollution Bulletin* **63**, 27–34.

Drucker, E. & Lauder, G. (2002), 'Experimental hydrodynamics of fish locomotion: Functional insights from wake visualization', *Integ. and Comp. Biol.* **42**, 243–257.

Dubrovinskaya, E. & Casari, P. (2019), Underwater direction of arrival estimation using wideband arrays of opportunity, *in* 'OCEANS 2019 - Marseille', pp. 1–7.

Dunt, T., Heck, K., Lyons, K., Murphy, C., Cal, R. & Franck, J. (2024), 'Wavelength-induced shedding frequency modulation of seal whisker inspired cylinders', *Bioinspir. Biomim.* **19**, 036004.

Elshalakani, M., Muthuramalingam, M. & Bruecker, C. (2020), 'A deep-learning model for underwater position sensing of a wake's source using artificial seal whiskers.', *Sensors* **20**, 3522.

Estebanez, L., El Boustani, S. & Destexhe, A. (2012), 'Correlated input reveals coexisting coding schemes in a sensory cortex', *Nature Neuroscience* **15**, 1691–1699.

Fang, B. (1990), 'Simple solutions for hyperbolic and related position fixes', *IEEE Transactions on Aerospace and Electronic Systems* **26**(5), 748–753.

Geyer, M. & Daskalakis, A. (1998), Solving passive multilateration equations using bancroft's algorithm, *in* '17th DASC. AIAA/IEEE/SAE. Digital Avionics Systems Conference. Proceedings (Cat. No.98CH36267)', Vol. 2, pp. F41/1–F41/8 vol.2.

Glick, R., Muthuramalingam, M. & Brücker, C. (2021), 'Fluid-structure interaction of flexible whisker-type beams and its implications for flow sensing by pair-wise correlation', *Fluids* **6(3)**, 102.

Glick, R., Muthuramalingam, M. & Brücker, C. (2022), 'Sea lions could use multilateration localization for object tracking as tested with bio-inspired whisker arrays', *Scientific Reports* **12**, 2045–2322.

Gomez, V., Remmas, W., Hernando, M., Ristolainen, A. & Rossi, C. (2024), 'Bioinspired whisker sensor for 3d mapping of underground mining environments', *Biomimetics* **9**(2).

Gong, P., Suresh, D. & Jin, Y. (2023), 'Coupling between vortex flow and whisker sensor in cylinder wakeswith time-varying streamwise gaps', *Phys. Rev. Fluids* **8**, 034701.

Grant, R. A. & Goss, V. G. A. (2022), 'What can whiskers tell us about mammalian evolution, behaviour, and ecology?', *Mammal Review* **52**(1), 148–163.

Hanke, W. & Bleckmann, H. (2004), 'The hydrodynamic trails of lepomis gibbosus (centrarchidae), colomesus psittacus (tetraodontidae) and thysochromis ansorgii (cichlidae) investigated with scanning particle image velocimetry', *J. Exp. Biol.* **207**, 1585–1596.

Hanke, W., Witte, M., Miersch, L., Brede, M., Oeffner, J., Michael, M., Hanke, F., Leder, A. & Dehnhardt, G. (2010), 'Harbor seal vibrissa morphology suppresses vortex-induced vibrations', *Journal of Experimental Biology* **213**(15), 2665–2672.

Hannah, D. M. & Garner, G. (2015), 'River water temperature in the united kingdom: Changes over the 20th century and possible changes over the 21st century', *Progress in Physical Geography: Earth and Environment* **39**(1), 68–92.

Heo, J., Chung, J. & Lee, J. (2006), 'Tactile sensor arrays using fiber bragg grating sensors', *Sens. Actuator A Phys.* **126 (2)**, 312–327.

Hollenbeck, A., Grandhi, R., Hansen, J. & Pankonien, A. (2023), 'Bioinspired artificial hair sensors for flight-by-feel of unmanned aerial vehicles: A review', *AIAA J.* pp. 1–26.

Jadhav, S. & Feldman, D. (2010), 'Texture coding in the whisker system', *Curr. Opin. Neurol.* **20**, 313–318.

Kamat, A. M., Zheng, X., Bos, J., Cao, M., Triantafyllou, M. S. & Kottapalli, A. G. P. (2024), 'Undulating seal whiskers evolved optimal wavelength-to-diameter ratio for efficient reduction in vortex-induced vibrations', *Advanced Science* **11**(2), 2304304.

Kent, T. A., Kim, S., Kornilowicz, G., Yuan, W., Hartmann, M. J. Z. & Bergbreiter, S. (2021), 'Whisksight: A reconfigurable, vision-based, optical whisker sensing array for simultaneous contact, airflow, and inertia stimulus detection', *IEEE Robotics and Automation Letters* **6**(2), 3357–3364.

Knapp, C. H. (1976), 'The generalized correlation method for estimation of time delay.', *IEEE Trans Audio Speech Lang Process* **24(4)**, 320–327.

Kogan, I. et al. (2015), 'The invisible fish: hydrodynamic constraints for predator-prey interaction in fossil fish saurichthys compared to recent actinopterygians', *Biol Open* **4(12)**, 1715–1726.

Krause, L. O. (1987), 'A direct solution to gps-type navigation equations', *IEEE Transactions on Aerospace and Electronic Systems* **AES-23**(2), 225–232.

Krüger, Y., Hanke, W., Miersch, L. & Dehnhardt, G. (2018), 'Detection and direction discrimination of single vortex rings by harbour seals (phoca vitulina)', *J. Exp. Biol.* p. 221.

Kundu, T. (2014), 'Acoustic source localization', *Ultrasonics* **54**(1), 25–38.

Leclercq, T. & de Langre, E. (2018), 'Vortex-induced vibrations of cylinders bent by the flow', *Journal of Fluids and Structures* **80**, 77–93.

Liao, Q., Wang, B. & Wang, P. (2015), 'In situ measurement of sediment resuspension caused by propellerwash with an underwater particle image velocimetry and an acousticdoppler velocimeter', *Flow Meas Instrum* **41**, 1–9.

Liu, G., Jiang, W., Zheng, X. & Xue, Q. (2021), 'Flow-signal correlation in seal whisker array sensing', *Bioinspir. Biomim.* **17**(1), 016004.

Liu, G., Jiang, Y., Wu, P., Ma, Z., Chen, H. & Zhang, D. (2022), 'Artificial whisker sensor with undulated morphology and self-spread piezoresistors for diverse flow analyses', *Soft Robotics* **0**.

Liu, J., Xu, P., Liu, B., Xi, Z., Li, Y., Guo, L., Guan, T., Zhu, P., Meng, Z., Wang, S., Wang, H. & Xu, M. (2024), 'Underwater biomimetic lateral line sensor based on triboelectric nanogenerator for dynamic pressure monitoring and trajectory perception', *Small* **20**(19), 2308491.

Luke, R. & McAlpine, A. (2019), A spiking neural network approach to auditory source lateralisation, *in* 'ICASSP 2019 - Brighton', pp. 1488–1492.

Lyons, K., Murphy, C. T. & Franck, J. A. (2020), 'Flow over seal whiskers: Importance of geometric features for force and frequency response', *PLOS ONE* **15**, 1–25.

Mannini, C., Marra, A. & Bartoli, G. (2014), 'Viv–galloping instability of rectangular cylinders: Review and new experiments', *J. Wind. Eng. Ind. Aerodyn.* **132**, 109–124.

Miersch, L. et al. (2011), 'Flow sensing by pinniped whiskers', *PTRBAE* **366**, 3077–3084.

Mills, A. W. (1958), 'On the minimum audible angle', *The Journal of the Acoustical Society of America* **30**, 237.

Milne, A., Smith, C., Orton, L., Sullivan, M. & Grant, R. (2020), 'Pinnipeds orient and control their whiskers: a study on pacific walrus, california sea lion and harbor seal', *Journal of Comparative Physiology* **206**, 441–451.

Morita, T., Kang, H., Wolfe, J., Jadhav, S. & Feldman, D. (2011), 'Psychometric curve and behavioral strategies for whisker-based texture discrimination in rats', *PloS one* **6(6)**, e20437.

Mortsiefer, C. & Peissig, J. (2017), Design of a ceiling-microphone array for speech applications with focus on transducer arrangements and beamforming techniques, *in* 'DAGA 2017 Kiel', pp. 544–547.

Murphy, C. T., Reichmuth, C. & Mann, D. (2015), 'Vibrissal sensitivity in a harbor seal (Phoca vitulina)', *Journal of Experimental Biology* **218**(15), 2463–2471.

Muthuramalingam, M. & Brücker, C. (2019), 'Seal and sea lion whiskers detect slips of vortices similar as rats sense textures', *Sci. Rep.* **9**, 12808.

Müller, U., Van Den Heuvel, B., Stamhuis, E. & Videler, J. (1997), 'Fish foot prints: Morphology and energetics of the wake behind a continuously swimming mullet (chelon labrosus risso)', *J. Exp. Biol* **200**, 2893–2906.

Nagy, A. (2016), Multilateration and kalman filtering techniques for stealth intelligence surveillance and reconnaissance using multistatic radar, Master's thesis, Carleton University, ON, Canada.

Niri, E. D. & Salamone, S. (2012), 'A probabilistic framework for acoustic emission source localization in plate-like structures', *Smart Materials and Structures* **21**(3), 035009.

Okello, N., Fletcher, F., Musicki, D. & Ristic, B. (2011), 'Comparison of recursive algorithms for emitter localisation using tdoa measurements from a pair of uavs', *IEEE Trans Aerosp Electron Syst* **47(3)**, 1723–1732.

Ollivier, B., Pepperell, A., Halstead, Z. & Hioka, Y. (2019), 'Noise robust bird call localisation using the generalised cross-correlation with phase transform in the wavelet domain', *JASA* **146**(6), 4650–4663.

Pal, S. et al. (2004), 'Strain-independent temperature measurement using a type-I and type-iia optical fiber bragg grating combination.', *Review of Scientific Instruments* **75(5)**, 1327–1331.

Ptak, M., Choiński, A. & Kirviel, J. (2016), 'Long-term water temperature fluctuations in coastal rivers (southern baltic) in poland', *Bulletin of Geography. Physical Geography Series* (11), 35–42.

Quist, B. W., Faruqi, R. A. & Hartmann, M. J. (2011), 'Variation in young's modulus along the length of a rat vibrissa', *Journal of Biomechanics* **44**(16), 2775–2781.

Raffel, M. et al. (2007), *Particle image velocimetry: a practical guide*, Springer Verlag, Berlin, Heidelberg, New York.

Rente, B. et al. (2021), 'Extended study of fiber optic-based humidity sensing system performance for sewer network condition monitoring', *IEEE Sensors Journal* **21(6)**, 7665–7671.

Schulte-Pelkum, N., Wieskotten, S., Hanke, W. et al. (2007), 'Tracking of biogenic hydrodynamic trails in harbour seals (phoca vitulina)', *J. Exp. Biol.* **210**, 781–787.

Takei, K. et al. (2014), 'Highly sensitive electronic whiskers based on patterned carbon nanotube and silver nanoparticle composite films', *PNAS* **111(5)**, 1703–1707.

Valdivia y Alvarado, P., Subramaniam, V. & Triantafyllou, M. (2012), Design of a bio-inspired whisker sensor for underwater applications, *in* 'SENSORS, 2012 IEEE', pp. 1–4.

Videler, J., Muller, U. & Stamhuis, E. (1999), 'Aquatic vertebrate locomotion: wakes from body waves', *J. Exp. Biol* **202**, 3423–3430.

Wang, J., Yang, X., Wang, A., Jiang, H., Bai, L., Meng, H., Li, S., Geng, T. & Sun, W. (2023), 'Bio-inspired fiber attitude sensor for direction-distinguishable pitching and rolling sensing', *Journal of Lightwave Technology* **41**(21), 6844–6851.

Wang, S. et al. (2023), 'Potential applications of whisker sensors in marine science and engineering: A review.', *J. Mar. Sci. Eng.* **11**, 2108.

Wieskotten, S., Dehnhardt, G., Mauck, B., Miersch, L. & Hanke, W. (2010), 'The impact of glide phases on the trackability of hydrodynamic trails in harbour seals (phoca vitulina)', *J. Exp. Biol.* **213**, 3734–3740.

Woolsey, T. A., Welker, C. & Schwartz, R. H. (1975), 'Comparative anatomical studies of the sml face cortex with special reference to the occurrence of "barrels" in layer iv', *Journal of Comparative Neurology* **164**(1), 79–94.

Xu, P. et al. (2021), 'A triboelectric-based artificial whisker for reactive obstacle avoidance and local mapping', *Research* **2021**.

Zhang, X. et al. (2021), 'Harbor seal whisker inspired self-powered piezoelectric sensor for detecting the underwater flow angle of attack and velocity', *IMEKO* **172**, 180866.

Zhao, C., Jiang, Q. & Li, Y. (2017), 'A novel biomimetic whisker technology based on fiber bragg grating and its application', *Meas. Sci. Technol.* **28**, 095104.

Zheng, X. (2022), Flow-sensing mechanisms and biomimetic potential of seal whiskers, PhD thesis, University of Groningen.

Zheng, X., Kamat, A. M., Cao, M. & Kottapalli, A. G. P. (2021), 'Creating underwater vision through wavy whiskers: a review of the flow-sensing mechanisms and biomimetic potential of seal whiskers', *Journal of the Royal Society Interface* **18**(183), 20210629.

Zheng, X., Kamat, A. M., Cao, M. & Kottapalli, A. G. P. (2023), 'Wavy whiskers in wakes: Explaining the trail-tracking capabilities of whisker arrays on seal muzzles', *Advanced Science* **10**(2), 2203062.